Numerical Study of the Structural Performance of Strong Wood Light-frame Shear Walls Under Large Lateral Loads

by:
Dina Ghazinader

A Thesis Submitted in Partial Fulfillment of the Requirements for the Degree of Master of Applied Science in the Department of Civil Engineering

Numerical Study of the Structural Performance of Strong Wood Light-frame Shear Walls Under Large Lateral Loads

by:

Dina Ghazinader

Supervisory committee :

Sardar Malek, Supervisor

Department of Civil Engineering

Min Sun, Co-supervisor

Department of Civil Engineering

Abstract

The motivation for this study comes from the increasing demand for safe, affordable wood-frame buildings in Canada over the past decade, primarily due to their low cost, high ductility, and ease of construction. In such buildings, wood-frame shear walls are commonly utilized as the main lateral load-resisting system to resist seismic loads. Wood-frame shear walls are typically comprised of timber framing members, sheathing panels such as plywood or oriented strand board (OSB), and fasteners like nails and bolts. The best performance of such walls is achieved when most of the energy is dissipated through shear deformation in the sheathing-to-framing connectors (i.e. nails) while the framing and anchorage systems remain in their elastic regime. This study presents the results of extensive numerical and analytical investigations into the behavior of "strong" wood-frame walls subjected to large monotonic and cyclic loads. A detailed 3D finite element (FE) model in ABAQUS software was employed for an in-depth analysis of shear wall components and to examine the impact of various parameters on their performance. The accuracy of the FE model for both the nail connectors and the wall assembly is validated by comparing its results with experimental data from the literature. Further analyses showed that the Canadian Standards Association (CSA), and the Special Design Provisions for Wind and Seismic (SDPWS) guidelines slightly overestimate the initial wall stiffness, with the discrepancy increasing at larger displacements. The numerical analyses conducted on strong shear walls with different hold-down systems show that discrete hold-down system can overstress the end studs, increasing the risk of wood crushing and brittle failure in the framing members.

In contrast, continuous steel rods maintain stresses within safe limits and shift the failure mode (nail yielding) from the end studs to the center of the wall, thereby enhancing the overall structural performance. The numerical results further indicate that, although the diameter of continuous rod hold-downs does not significantly affect the wall's strength, it plays a critical role in delaying yielding in the anchorage system, thereby improving the overall wall performance and energy dissipation under lateral loads. Numerical results also show that thicker OSB sheathing panels or materials with a higher modulus of elasticity (MOE) improves energy dissipation while ensuring the frame members and anchorage system remain within their elastic range. Thicker panels help prevent edge tear-out and nail head pull-through by reducing the crushing of wood strands in the OSB, allowing the nails to deform more before ultimately withdrawing. This suggests that optimizing the mechanical properties of sheathing panels may improve shear wall performance and energy dissipation while minimizing the need for additional nails, providing a balanced approach to enhancing both strength and ductility in the design leading to more resilient shear walls under strong earthquakes.

Contents

List of Figures

List of Tables

Acknowledgments

I am deeply thankful to everyone who supported me throughout this research project. Your guidance and encouragement were invaluable in helping me overcome challenges. Your help has been instrumental in making this work possible—thank you.

To my supervisor, Sardar Malek, for trusting my capabilities and providing me with this opportunity. Your guidance has been invaluable, teaching me not only to think creatively and critically but also that true success comes with humility and kindness. Thank you for inspiring me and for being an exceptional role model throughout this journey.

To my co-supervisor, Min Sun, who has been an unwavering source of support and guidance throughout this project. Thank you for your patience, encouragement, and for always challenging me to strive for excellence.

I am also sincerely grateful to Dr. J. Daniel Dolan for his technical feedback and for providing UEL subroutine sources for cyclic modeling, Dr. Xavier Estrella for providing experimental data on shear walls with continuous rods, and fruitful discussion with Dr. Chun Ni (FPInnovations) on codes and standards.

I would like to acknowledge the financial support from the University of Victoria (FGS Award).

I wish to express my deepest gratitude to my parents, Monireh and Nader, for being my greatest support over the past two years. You stood by me every step of the way, pushing me forward when times were tough. Thank you for teaching me the importance of hard work, the value of humility, and the strength to never give up.

To my siblings, Donya and Sina, thank you for always being there through the highs and lows. I owe it all to you.

To my friends, thank you for your encouragement, laughter, and for helping me stay grounded throughout this journey.

1 Introduction

1.1 General

Over the past few decades, there has been a remarkable rise in the use of wood light-frame structures for low-rise construction in North America, Europe, and Oceania. Due to advancements in building technology and the development of engineered wood products, the height limit for wood light-frame buildings in Canada's provincial and national building codes (NBCC) has been raised from 4 to 6 stories since 2009 [1]. Meanwhile, according to the 2015 and 2020 editions of the National Building Code of Canada (NBCC), the seismic design spectra have been significantly increased for all site classes to account for updated seismic hazard assessments and improved ground motion prediction models, ensuring that buildings are designed to better withstand potential seismic forces and enhance public safety [1, 2]. As a result, there is a greater need for higher lateral load resistance in mid-rise wood light-frame buildings, especially in high seismic zones.

Wood light-frame shear walls are critical in providing this resistance, as they play a crucial role in resisting the lateral loads generated by wind or seismic forces. A typical wood light-frame shear wall consists of a wood frame with 38 × 89 mm (2" × 4") interior studs, spaced at 400 mm on center, double end studs, single members for the bottom and top plate, and conventional corner hold-downs to prevent overturning [3]. The schematic configuration of a wood light-frame shear wall is shown in Figure 1. As buildings increase in height, the need for stronger wood light-frame shear walls (higher capacity assemblies) becomes more critical to withstand increased gravitational and seismic forces. This 'strong' configuration, characterized by 38 × 135 mm (2" × 6") framing members, sturdy end studs, stronger hold-down devices, OSB panels on both sides, and a smaller nail spacing [3]. The framing members provides a stand for attaching sheathing panels using nails or similar fasteners. These framing components resist vertical loads and out-of-plane forces. Meanwhile, the sheathing panels help withstand the in-plane lateral loads. The capacity of the wall is primarily determined by the strength of the fasteners connecting the sheathing to the studs. When these connections fail, they provide the building with the most ductile behavior, as this failure involves nail yielding and limited wood crushing [4–8].

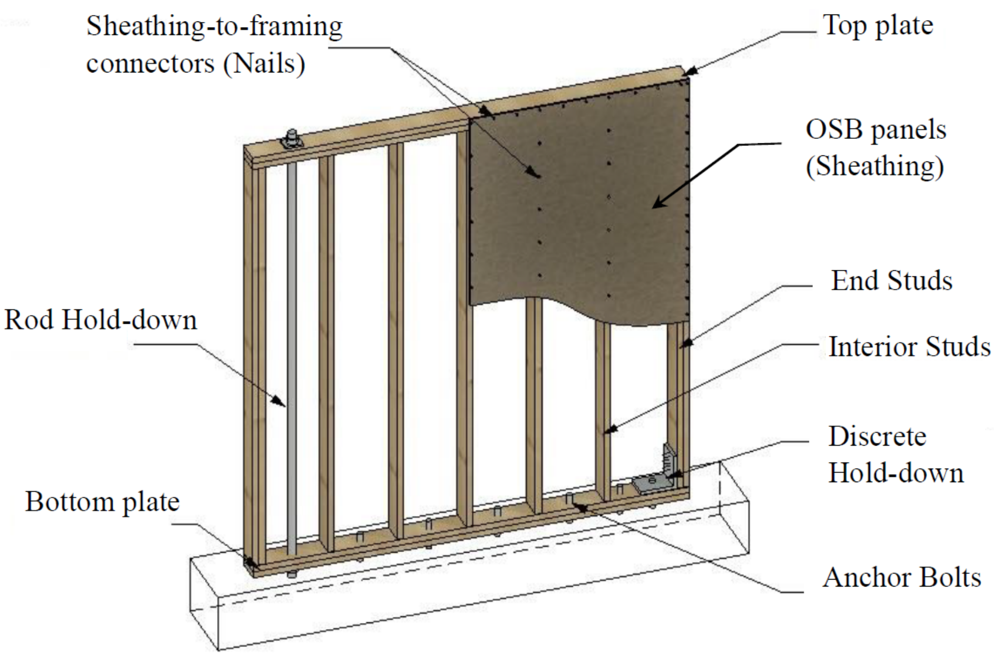

Figure 1: Schematic configuration of wood light-frame shear walls.

1.2 Motivation

The motivation behind this thesis arises from the increasing demand for safe and affordable wood light-frame buildings over the past decade. These buildings have become increasingly popular due to their low cost, high ductility, and ease of construction. In these structures, wood light-frame shear walls are commonly employed as the primary system for resisting seismic loads. Since 2009, the allowable height for wood light-frame buildings in Canada has risen from 4 to 6 stories. Additionally, national building codes have been updated with higher seismic design spectra to enhance building resilience and public safety. Consequently, there is a greater need for higher-capacity shear wall systems in mid-rise wood light-frame buildings, particularly in high seismic zones. This research aims to analyze the behavior of strong wood light-frame shear walls under large lateral loads, focusing on the structural performance of individual components. Various parameters have been evaluated to optimize the performance of shear walls while maintaining the integrity of the overall structural system.

1.3 Scope and limitations

This study presents the results of comprehensive numerical and analytical investigations into the behavior of strong wood-frame walls under large monotonic and cyclic loads using a 3D finite element (FE) model developed in ABAQUS software. By analyzing the structural performance of shear wall components, including wood members and nail connections, this research aims to optimize the performance of shear walls while ensuring that the framing and anchorage systems remain within their elastic limits.

The research is limited to single-story shear wall configurations and does not consider the multi-story structures, which are outside the scope of this study. Moreover, while thicker sheathing and increased modulus of elasticity are shown to improve energy dissipation, additional experimental work is needed to validate these findings. Additionally, further studies are needed to investigate the parameters affecting the cyclic response of shear walls.

1.4 Thesis structure

The thesis is structured as follows: It begins with an Introduction including scope and limitations. Following this is the Background and Literature Review, which covers experimental programs, analytical equations, and numerical modeling relevant to strong wood light-frame shear walls. The third chapter, Finite Element Modeling Approach, describes the shear wall specimens, material properties, and the types of elements used in the model. It also details the sheathing-to-framing connections, boundary conditions, loading protocols, and the validation of the model. Next, the Response Assessment chapter investigates the structural behavior of the walls, focusing on the components, connections, and the evaluation of analytical deflection equations. The fifth chapter presents Parametric Studies, examining the effects of various construction details on shear wall performance. In the Cyclic Analysis chapter, the focus shifts to modeling the behavior of the nail connections, loading protocols, and the validation of cyclic models. Finally, the thesis concludes with a Conclusions section, summarizing the key findings and contributions of the research.

2 Background and Literature Review

2.1 Experimental Programs

Before the mid-1940s, timber constructions relied on "let-in" corner bracing or diagonal lumber sheathing for lateral resistance against wind and earthquake forces [8], as depicted in Figure 2. Panel sheathing began to be implemented for shear walls in the late 1940s. The established procedure for testing shear wall panels in North America is outlined in the American Society of Testing Materials E72-77 [9]. This standard serves as the testing protocol for determining the racking resistance of shear walls, influencing the building codes across North America. Tissel [10] utilized the ASTM E72-77 test to assess the comparative effectiveness of plywood-sheathed shear walls and those with let-in diagonal corner bracing. The results from tests conducted on 2.4 x 2.4 m (8 x 8 ft) shear walls revealed that walls partially sheathed with plywood exhibit an ultimate load capacity comparable to that of let-in corner braced walls. These findings, combined with studies conducted by Tissel and Eliott [11] for diaphragms and Adams [12] for shear walls, served as the foundation for determining the allowable shear capacities in the building codes of the United States.

Several studies have established that the major contributor to wood light-frame shear wall's deflection is nail slip, and a significant improvement in the ultimate loading capacity can be achieved by reducing the nail spacing [13–15]. Dolan and Madsen [16] tested 11 full-scale wood light-frame shear walls to investigate their monotonic and cyclic behavior. The results demonstrated the significant influence of the nail connections between the sheathing and the framing on the load-displacement characteristics of the shear walls. The study confirmed that the hysteresis of the shear walls is contained within an envelope defined by the monotonic load-displacement curve. A high-capacity shear wall system with two or three rows of nails was developed and tested by Qiang et al. [17], showing that lateral load resistance increases proportionally with the number of nail rows. These walls demonstrated greater initial stiffness and ultimate displacement than standard shear walls, but their duc-

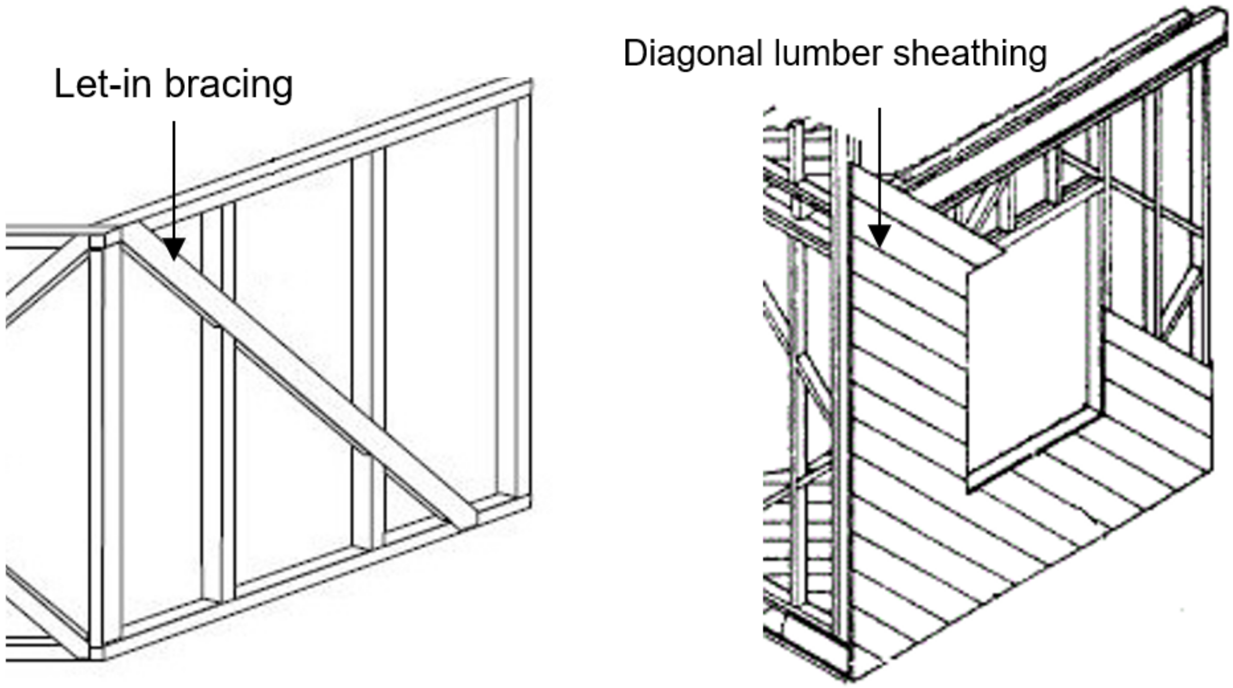

Figure 2: Corner bracing "let-in" or diagonal lumber sheathing for lateral resistance [8].

tility was lower. This reduction in ductility was attributed to sheathing buckling and stud splitting, which limited the ultimate displacement.

Several research studies have contributed to the refinement of design expressions and values related to the stiffness and strength specified in the Design Provisions. Griffits [18] conducted a thorough series of shear wall tests with the aim of developing a practical and precise design approach for timber frame shear walls subjected to in-plane shear forces. These tests involved various sheathing panel materials. This comprehensive examination of test data led to the formulation of two empirical design methods, contributing valuable insights to the field. To acquire a representative dataset supporting a design methodology, Salenkovich and Dolan [19] conducted tests on typical wood light-frame shear walls with varying aspect ratios. These tests involved applying both monotonic and cyclic in-plane shear loads, with standard OSB panels as the sheathing material. A similar investigation was carried out by the NAHB Research Center [20], where fiberboard was used as the sheathing material. In an experiment conducted by Martin [21], 89 shear walls with various configurations and aspect ratios were tested to compare the measured deflection with calculations based on the design standard equation [22]. The results revealed that the design equation typically underestimated the wall deflection.

Kamiya et al. [23] carried out a study investigating how wall length affects the lateral resistance of shear walls. By adjusting the aspect ratios from 1/3 to 2 and utilizing plywood sheathing, they found that as wall length increases, shear strength increases proportionally. Lam et al. [24] examined shear walls with nonstandard large OSB panels (2.4×7.3 m) and standard size OSB panels (1.2×2.4 m). Walls with nonstandard panels showed a significant 36% increase in stiffness and a 30% increase in strength. Ductility ratios were consistent for both panel sizes, but walls with standard panels dissipated more energy under cyclic loads compared to those with large panels. An experimental campaign was conducted by Byloos and Vandoren [25] to enhance the understanding of the behavior of wood light-frame shear walls with double-layered sheathing panels on one side of the framing. They tested eight full-scale configurations under monotonic loading. The sheathing materials used included both load-bearing and non-load-bearing gypsum plasterboards, as well as particle boards. Each sheathing panel had a thickness of 12.5 mm. The results showed that adding a second sheathing layer of the same material, using the same fastener arrangement as the inner layer, does not fully double the racking capacity or stiffness. The most noticeable increase in stiffness, from 661 N/mm to 968 N/mm, was observed when a second load-bearing plasterboard layer was added. Adding a non-load-bearing inner layer most notably affected the post-peak behavior, resulting in a more ductile failure compared to single-layered walls or walls with load-bearing inner layers. He et al. [26] introduced a novel design for PVC wood-plastic composite wall panels, using PVC composites as facing panels and Spruce-Pine-Fir lumber as the framework, connected by self-tapping screws. Two panel specimens were tested under monotonic and cyclic loading, and finite element (FE) models, using beam and shell elements, were created in ANSYS Workbench to assess lateral performance. The experimental and numerical results demonstrated that the panels exhibit good shear strength, and lateral deformation properties. The nail connection specimens showed 1.75 to 2.16 times the strength and over three times the displacement of the 15.1 mm OSB panels. These findings suggest that PVC wood-plastic composite panels hold promise for use as shear walls in structural applications.

Hold-down anchorages play a crucial role in wood light-frame shear walls. Lebeda et al. [27] discovered that relocating hold-downs to the first interior stud, rather than the end stud, resulted in a significant reduction in average strength (42% in monotonic tests, 35% in cyclic tests). This shift caused non-typical failures, including hold-down fastener failure, bottom plate splits, and diminished wall energy dissipation. Johnston et al. [28] conducted tests on twenty-one shear walls, some of which were equipped with hold-down anchors, while others were not. Hold-down anchors showed minimal impact on lateral strength, stiffness, and energy dissipation for walls experiencing vertical loads between 12 kN/m and 25 kN/m. In an investigation by Bagheri [29], two conventional (non-strong) wood light-frame walls with continuous rod hold-downs were subjected to monotonic load, and their performance was contrasted with walls featuring discrete hold-downs. The findings indicated that the utilization of continuous hold-downs led to enhancements in strength (13.8%), stiffness (17.1%), and ductility (21.5%) of the walls. However, the overall influence on the specimens' response was not particularly pronounced, as the lateral behavior of the walls was predominantly influenced by the sheathing-to-framing connectors.

Guíñez et al. [5] examined the lateral performance of strong wood light-frame walls with discrete hold-downs under both monotonic and cyclic loading, with variations in wall length and nail spacing. Their findings revealed that these walls demonstrate greater capacity and delayed stiffness degradation. Additionally, the study indicates that smaller nail spacing significantly enhances strength and postpones stiffness degradation. Estrella et al. [4] conducted an experimental and numerical investigation into the behavior of strong shear walls with continuous rod hold-downs subjected to lateral loads. Four different wall configurations were tested, comparing those with continuous rod systems to those with discrete hold-downs. Results indicate that walls with continuous rods exhibit 35.8 percent higher strength, remaining elastic up to drifts of about 0.8%. However, there was notable stiffness degradation during testing, with residual stiffness averaging around 15-20% of the initial value. Additionally, a nonlinear model was developed to further examine the tested specimens, revealing a unique failure pattern concentrating damage on nails at the central studs of the wall.

2.2 Analytical Equations

A mechanics-based approach to describe the deformation behavior of wood light-frame shear walls was first formulated in 1952 [30]. During the formulation of the deflection equation, six quarter-scale and four full-scale diaphragm specimens underwent testing. The original equation developed closely resembles the one featured in the current Canadian wood design standard [31], except for the exclusion of the hold-down elongation contribution.

The Canadian standard [31] provides an equation that involves four terms for calculating the static deflection of a blocked shear wall segment. The general format of the deflection equation is presented in Equation 1.

$$\Delta_t = \Delta_b + \Delta_s + \Delta_n + \Delta_a \tag{1}$$

where, Δ_b is the total horizontal deflection of the wall, Δ_b is the bending deflection of the wall, Δ_s is the panel shear deformation, Δ_n is the horizontal deflection caused by nail slip and Δ_a is the horizontal deflection caused by hold-down elongation.

For a cantilever wall with a concentrated load applied at the free end, as shown in Figure 3, the bending deflection can be described by Equation 2.

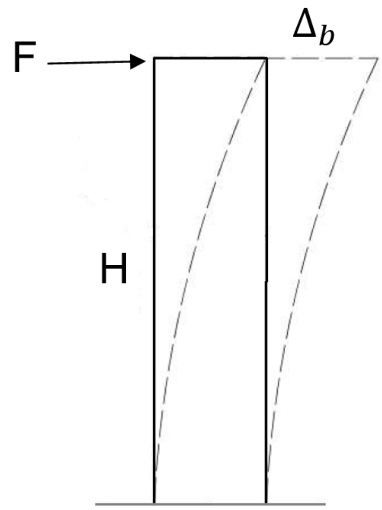

Figure 3: Bending term of the equation

$$\Delta_b = \frac{FH^3}{3EI} \tag{2}$$

Where, F is the concentrated load at the free end, H is the height of the wall, E is the wall modulus of elasticity, and I is the moment of inertia of the wall. The total force on the wall is calculated by multiplying the uniform diaphragm force by the wall length, as demonstrated in Equation 3. The moment of inertia of the wall is described by Equation 4.

$$F = \nu \times L \tag{3}$$

$$I = \frac{AL^2}{2} \tag{4}$$

Therefore, bending deflection can be expressed as shown in Equation5.

$$\Delta_b = \frac{2\nu H^3}{3EAL} \tag{5}$$

where, ν (N/mm) is maximum shear force per unit length, H is shear wall height (mm), E (N/mm^2) is the longitudinal modulus of elasticity of the end studs, A (mm^2) is the cross-section area of end studs, L is length of the wall. The deflection due to panel shear deformation can be written as shown in Equation 6. where, B_ν (N/mm) is shear through thickness rigidity of the sheathing. The shear deformation due to panel deformation is illustrated in Figure 4.

$$\Delta_s = \frac{\nu H}{B_\nu} \tag{6}$$

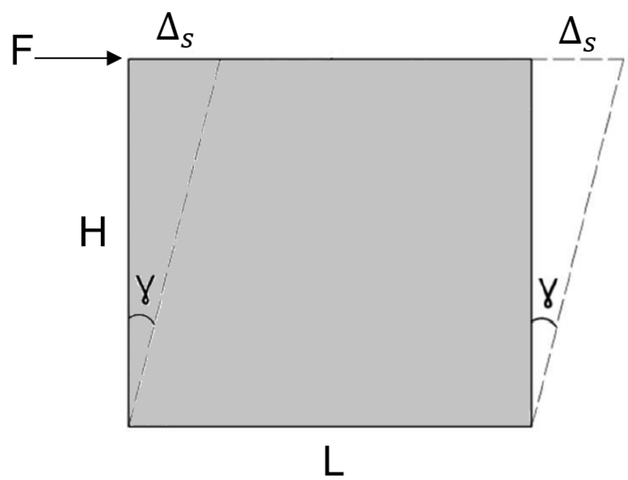

Figure 4: Shear term of the equation

γ represents the shear strain of the panel, which is formulated as shown in Equation 7.

$$\gamma = \frac{\Delta_s}{H} \tag{7}$$

Equation 8 has been proposed to estimate the deflection due to nail slip.

$$\Delta_n = 0.0025 H e_n \tag{8}$$

While the nail slip equation was originally developed for diaphragms, it can be applied to shear walls with appropriate assumptions. In this context, equal strain across nails at panel edges is assumed, despite known variations where corner nails experience higher forces and exhibit increased deformation. This assumption provides a reasonable average estimate of the nail slip component. The Canadian wood design standard contains an empirical equation to estimate the sheathing-to-framing connection deformation (nail slip) as expressed in Equation 9.

$$e_n = \left(\frac{0.013\nu_s}{d_f^2}\right)^2 \tag{9}$$

where, ν (N/mm) i maximum specified shear force per unit length along the top of the shear wall load, S (mm) is nail spacing along the panel edges, and d_f (mm) is the nail diameter.

The final term in the deflection equation considers the rigid body rotation of the wall. The horizontal wall deflection due to the uplift which is depicted in Figure 5 is a function of the vertical elongation due to the rigid body rotation multiplied by the wall's aspect ratio, as shown in Equation 10.

$$\Delta_a = \frac{Hd_a}{L} \tag{10}$$

For shear wall segments without hold-downs, the Canadian wood design standard provide an equation to calculate the to total vertical elongation (d_a) . When a hold-down is provided, d_a can be obtained from the manufacturer since it highly depends on the hold-down system used.

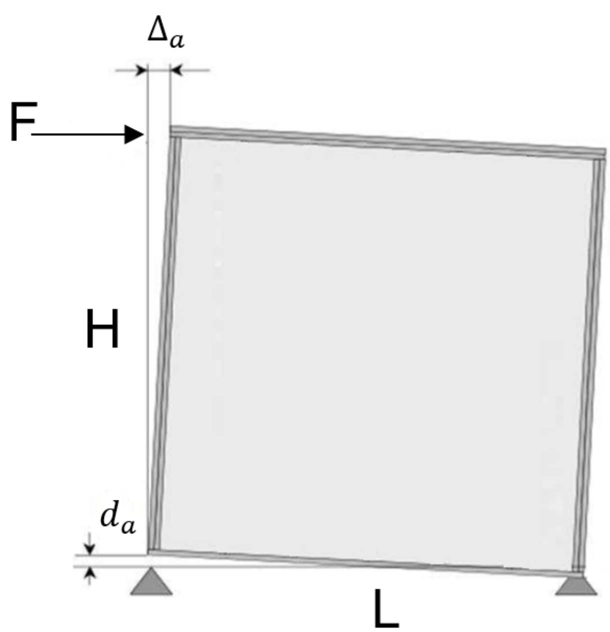

Figure 5: Wall rigid body rotation

The total shear wall deflection can be expressed as Equation 11:

$$\Delta_t = \frac{2\nu H^3}{3EAL} + \frac{\nu H}{B_\nu} + 0.0025He_n + \frac{Hd_a}{L} \tag{11}$$

A similar expression to Canadian design standard can be found in the American Wood Council (AWC) 2021 SDPWS [32]. Although the background for the expression is the same as the Canadian design standard, there are some differences. The shear wall deflection in SDPWS, δ_{sw} , is calculated using the following equation (Equation 12):

$$\delta_{\text{sw}} = \frac{8\nu h^3}{EAb} + \frac{\nu h}{1000G_a} + \frac{h\Delta_a}{b} \tag{12}$$

where, b (mm) is shear wall length, ν (N/mm) is unit shear force induced by the design load, h (mm) is shear wall height, E (N/mm^2) is modulus of elasticity of end posts, A (mm^2) is area of end stud cross-sections, G_a (kips/in) is apparent shear wall shear stiffness from nail slip and panel shear deformation (which refers to an effective or simplified measure of the shear stiffness of a system), and Δ_a is vertical deformation of the wall overturning anchorage system.

The desired displacement is defined as the displacement corresponding to the nominal resistance provided based on each of the Standards. Nominal resistance is essential in structural design as it provides the baseline capacity of a material or structural member under standard, ideal conditions. It is used for calculating factored resistance by applying safety and adjustment factors, accounting for material variability, imperfections in construction, and uncertainties in load predictions. Adjustments for real-world conditions, such as duration of load, environmental effects, and size or system effects, ensure the design reflects actual performance. Nominal resistance is critical for assessing compliance with design standards like CSA O86 and the National Building Code of Canada, which require it for evaluating both ultimate and serviceability limit states. Based on CSA O86 Standard, the shear resistance (or nominal strength) of a shear wall segment with wood structural panels shall be calculated as follows:

$$V_{rs} = v_d J_D n_s J_{lus} J_s J_{hd} L_s \tag{13}$$

where, $v_d = N_u/s, N_u$ is lateral strength resistance of sheathing-to-framing connections along panel edges, s is fastener spacing along panel edges, J_D is the adjustment factor for diaphragm and shear wall construction, n_s is the number of shear planes in sheathing-to-framing connections, J_{lus} is the factor for unblocked shear walls, J_s is the fastener spacing adjustment factor, J_{hd} is the hold-down-effect factor for the shear wall segment, and L_s is the length of the shear wall segment parallel to the direction of load. The CSA O86 standard [3] provides detailed instructions for calculating each parameter. Additionally, the SDPWS design standard [2] offers nominal shear capacities for sheathed wood light-frame shear walls in tabular form, accounting for various factors. The investigation of shear walls with continuous rod hold-downs under lateral loads, conducted by Estrella et al. [4], revealed that current design guidelines underestimate wall strengths by 39.9% and overestimate stiffness by 37.5%. Casagrande et al. [33] developed a model through parametric studies to predict the behavior of walls with different geometries. The contributions of various components were assessed, and a simplified formula was introduced. The findings highlighted that the main contributors to wall deflection are the sheathing-to-framing connection, rigid body rotation, rigid body translation, and sheathing panel shear deformation.

2.3 Numerical Models

Due to the inherent complexity, expense, and time required for full-scale tests, along with the limitations of analytical models, virtual testing through numerical simulations provides a more practical solution for studying the behavior of wood light-frame walls. In recent decades, extensive research has been dedicated to developing models capable of accurately predicting the behavior of wood light-frame shear walls.

Given that the predominant factor influencing the wall's response is the nonlinear shear behavior of the connections between sheathing and framing [34], simple models, like the one proposed by Gupta and Kuo [35] which is a single-story wall with five degrees of freedom, prove effective in accurately predicting the overall force–displacement relationship. Folz and Filiatrault [36] developed a numerical model to predict the load-displacement response and energy dissipation of conventional wood shear walls with corner hold-downs under quasi-static cyclic loading. The model, implemented in the CASHEW program, accurately simulates wall behavior by incorporating rigid framing members, elastic sheathing panels, and nonlinear sheathing-to-framing connectors. Validation against full-scale tests showed that the model provides reliable predictions of load-displacement response which is shown in Figure 6. A revised version of the model was later suggested by Pang and Hassanzadeh [37]. The "Bouc-Wen-Baber-Noori (BWBN)" model [38], originally designed for both single-degree-of-freedom mechanical systems and multi-degree-of-freedom shear beam structural systems under forced vibration, was modified by Jian Xu and J. Daniel Dolan [39] to depict the hysteretic behavior of nailed connections. This model employs a set of ordinary differential equations to describe the hysteretic constitutive behavior. It can generate versatile and smoothly varying hysteresis curves, featuring nonlinearity, history dependency, and accounting for stiffness and strength degradation, as well as pinching of nail connections. Through the utilization of genetic algorithms and test data, suitable parameters for various joint configurations can be estimated. The model developed by Jian Xu and J. Daniel Dolan [39] was incorporated into the commercial software ABAQUS/Standard as a user-defined element, enabling accurate representation of the coupling effects in nail joints. It was then applied to the modeling and analysis of wood light-frame shear walls, showing reasonable agreement with experimental results in capturing the hysteresis loops.

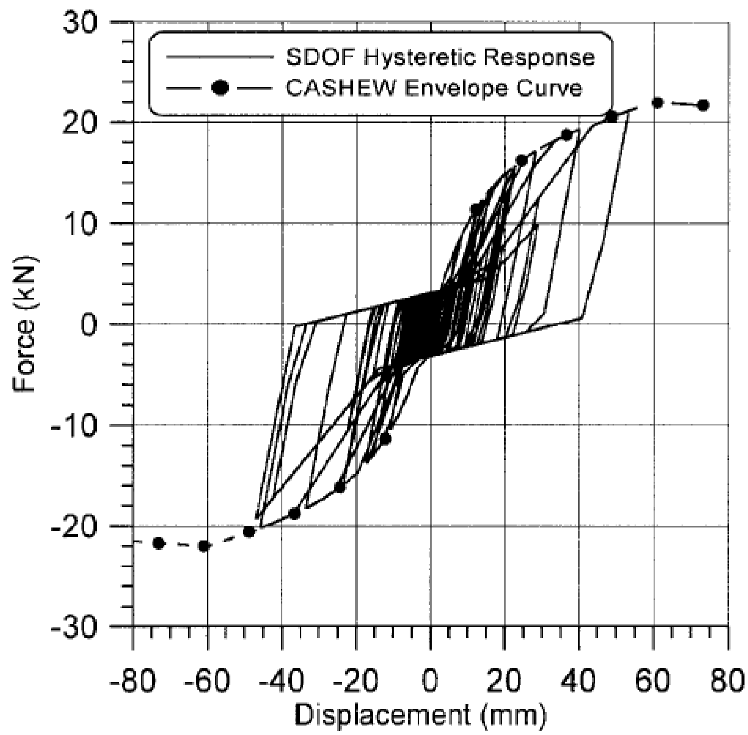

Figure 6: SDOF Model Prediction of Hysteretic Response of Shear Wall and Monotonic Envelope Curve Predicted by CASHEW. Figure is reproduced with permission from the source [36].

Estrella et al. [3] proposed an efficient nonlinear modeling approach to accurately simulate the seismic behavior of "strong" wood light-frame walls and demonstrate the differences in lateral response between such walls and conventional ones. Building on previous research efforts [36, 40, 41], the model aims to create a more inclusive approach that accurately predicts key behaviors, including force and stiffness degradation. It also showed that redesigning the nailing pattern can boost wall capacity by up to 10%, while anchorage demands remain safely below failure capacity. Additionally, the model was useful for calibrating simpler SDOF models to predict the dynamic behavior of mid-rise timber buildings.

In another work by Estrella et al. [4], experimental and numerical analyses were conducted on four wall configurations, each featuring varying diameters of continuous rod hold-downs and different nail spacing. These configurations were subjected to cyclic lateral loads and compared with traditional walls using discrete systems. The findings reveal that walls equipped with continuous rod systems exhibit a 35.8% increase in strength and maintain elasticity up to 0.8% drifts. Additionally, the study highlights discrepancies in the Special Design Provisions for Wind and Seismic (SDPWS), which underestimates wall strength by about 40% and overestimates stiffness by 37.5%. A detailed nonlinear model was developed to further investigate, uncovering a distinct failure pattern that concentrates damage at the nails of the central studs as depicted in Figure 7.

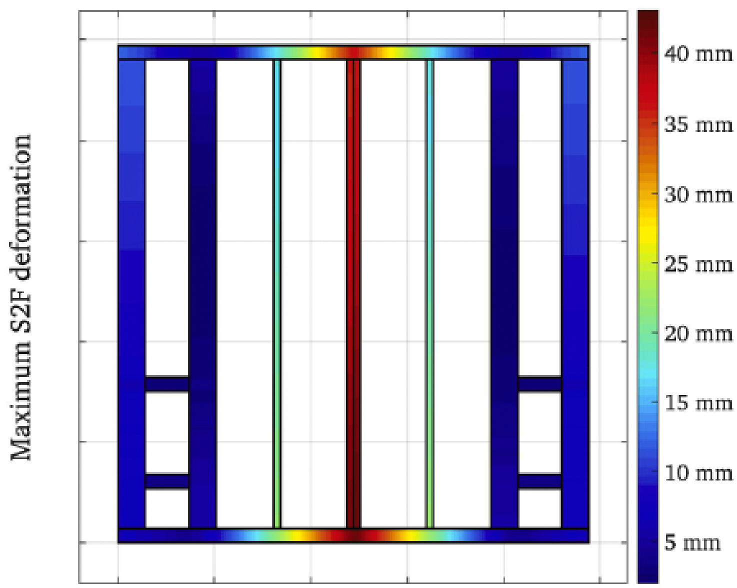

Figure 7: Deformation demand contour plots of nails for the wall with continuous rod hold-downs. Figure is reproduced with permission from the source [4].

3 Finite Element Modeling

3.1 General

Numerical models serve as powerful tools in engineering, offering a pathway to extend research beyond the confines of the laboratory. They provide a means to overcome the limitations, both physical and economic, of experimental testing, offering a virtual platform where various scenarios can be explored with relative ease. By accurately replicating the nonlinear behavior of structural systems, these models enable the management of uncertainties associated with testing full-scale structures. Furthermore, they offer valuable insights into test procedures, results, and findings. However, numerical models typically require validation against physical specimens to establish the expected accuracy levels essential in structural engineering. This validation becomes even more crucial when assessing new or innovative systems, ensuring alignment between theoretical predictions and empirical observations. This section presents a detailed numerical model for the strong wood light-frame shear walls developed within the commercial software ABAQUS [42]. This software offers robust capabilities for structural analysis, making it a suitable choice for the complexities involved in modeling wood light-frame shear walls. The model replicated the scale as well as the dimensional and mechanical properties of the elements in the test specimens. In the subsequent sections, the validation process of the numerical model against experimental data is outlined, followed by a thorough exploration of the insights obtained through the analyses conducted.

3.2 Description of strong shear wall specimens with Discrete and Continuous rod hold-downs

Shear wall specimens from experimental works performed by other researchers have been utilized [4, 5]. These specimens serve as references to validate the accuracy and efficacy of the numerical modeling approach developed in this study.

Guíñez, et al. [5] carried out seventeen in-plane monotonic and cyclic shear tests on wood light-frame shear walls with discrete hold-downs of various lengths (1200, 2400, and 3600 mm) and a height of 2470 mm. These walls were constructed using MGP10 graded Chilean radiata pine elements, including 35 × 138 mm (2" × 6") vertical studs spaced at 407 mm intervals, along with 2" × 6" double plates positioned at the top and bottom of the wall. The robust end studs comprised of five vertical studs each. Additionally, double vertical studs were placed at the edges of 1200 by 2400 11.1-mm thick APA rated OSB sheathing panels mounted on both faces of the wall to facilitate nailing. Nails with a diameter of 3×70 mm, spaced at 50 or 100 mm intervals, were utilized to attach the OSB panels to the frame elements. Simpson-Strong Tie HD12 hold-down anchors were secured with four 1×10 bolts to the sturdy end studs and with one 1–1/8×10 bolt to the foundation. To prevent wall sliding, 1×10 shear bolts were inserted through the bottom plate between vertical studs. Each specimen's hold-downs were bolted to a steel foundation beam to ensure stability and structural integrity. The schematic of the wall with a length of 2400 mm considered in this study is depicted in Figure 8(a).

Estrella et al. [4] tested four wood light-frame shear wall specimens with continuous rod hold-downs in various configurations under lateral cyclic loading. As illustrated in Figure. 8(b), the wall configuration comprised seven studs spaced at 400 mm intervals. Each end-stud consisted of four members. Both the bottom and top plates were composed of double members. All framing elements were constructed using 35 × 138 mm (2" × 6") dimensional lumber, employing mechanically graded MGP10 Chilean radiata pine. The studs were affixed to the bottom and top plates using steel nails, 3 mm in diameter and 100 mm in length. The walls were sheathed on both sides with 11.1 mm thick APA rated OSB panels, measuring 1220 mm in width and 2400 mm in height. These panels were vertically oriented and secured to the frame using spiral nails, 3 mm in diameter and 70 mm in length. Edge nailing was spaced at 50 or 100 mm intervals, while field nailing was spaced at 200 mm intervals. To prevent stress concentrations and wood crushing at the end-studs, edge nailing was evenly distributed among the four framing members. Simpson Strong-Tie continuous rod hold-downs were employed to anchor the wall to the foundation, which consisted of a reaction steel beam. The rods utilized were 12.7, 31.8, and 44.5 mm (1/2, 1–1/4, and 1–3/4) diameter threaded bars grade 105, with a yield strength of 724 MPa. Additionally, to replicate real installation conditions of continuous rod hold-downs, a 160 mm height timber floor was added on top of the wall. Consequently, the dimensions of the specimen were 2440 × 2600 mm (2440 × 2440 mm without the timber floor). Finally, four 25.4 mm diameter shear bolts were installed at the bottom plate to prevent lateral sliding of the wall. Documentation of the testing setup and additional details of the experimental results can be found in the references mentioned.

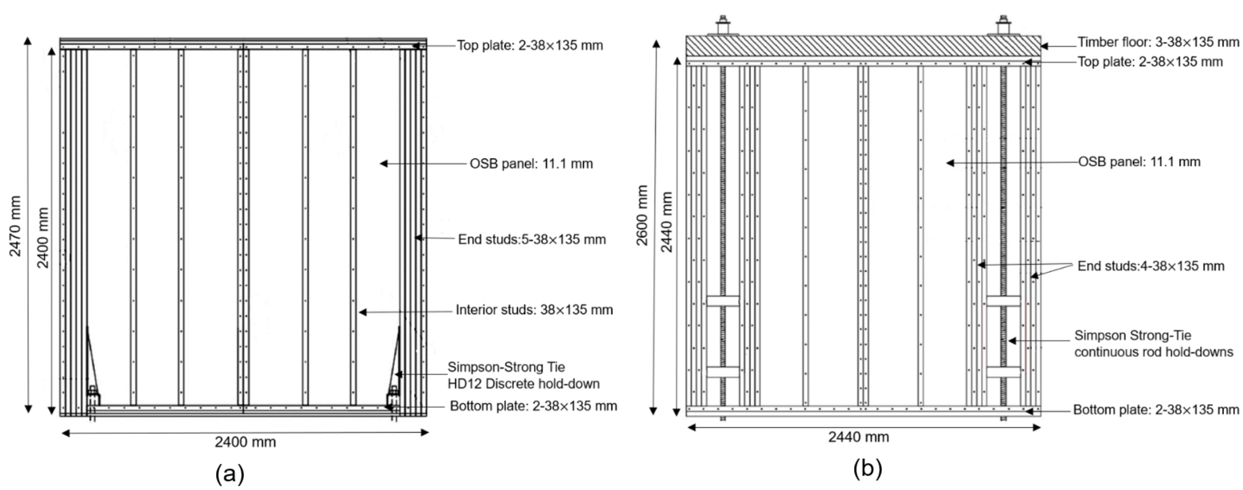

Figure 8: Configuration and components of the wood light-frame shear wall specimens : (a) with Discrete hold-downs, (b) with continuous rod hold-downs. Figure is reproduced with permission from the source [4, 5].

3.3 Material properties

The wooden frame utilized MGP10 graded Chilean radiata pine components (NCh1198 [43]), which closely resembles Southern Pine. From previous bending tests, a mean modulus of elasticity (E) of 11.4 GPa was assigned to the studs [3]. For the OSB shear tests, an average shear modulus (G) of 1.3 GPa was used as input for the model [3]. Elastic orthotropic material properties were assigned to all wood elements, as summarized in Table 1, and incorporated into ABAQUS for the frame components and OSB panels. To obtain the full set of orthotropic mechanical properties, additional data from Malek et al. [44, 45] and the Wood Handbook [46] were utilized.

Table 1: Material Properties for radiata pine framing and 11.1-mm-thick OSB panels used as input data for ABAQUS [3, 4, 44–46]. The units of Young's and shear moduli are GPa.

Material Property	**Framing members**	**OSB**
E_1 (GPa)	11.4	5.17
E_2 (GPa)	1.2	2.98
E_3 (GPa)	0.75	0.13
G_{12} (GPa)	0.869	1.255
G_{13} (GPa)	0.797	1.307
G_{23} (GPa)	0.142	0.128
ν_{12}	0.467	0.184
ν_{13}	0.456	0.364
ν_{23}	0.488	0.312

3.4 Element types employed in the model

The FE models are comprised of the stud, top plate, bottom plate, foundation, sheathing panels, stud-to-top and stud-to-bottom plate connection, and sheathing-to-frame connections. Two types of element models were assessed: solid element models, as well as beam and shell element models. Beam and shell element models offer simplicity compared to solid models and bring certain advantages, such as decreased solution time. However, they also come with limitations, such as the impact of material orientation, surface contact between different components, and the inability to capture through-thickness results, which solid element models can address. The effect of orthotropic material orientation for these two types of elements is discussed in Appendix A. Figure 9 illustrates the schematic of both element type models developed for wood light-frame shear walls used in the analysis.

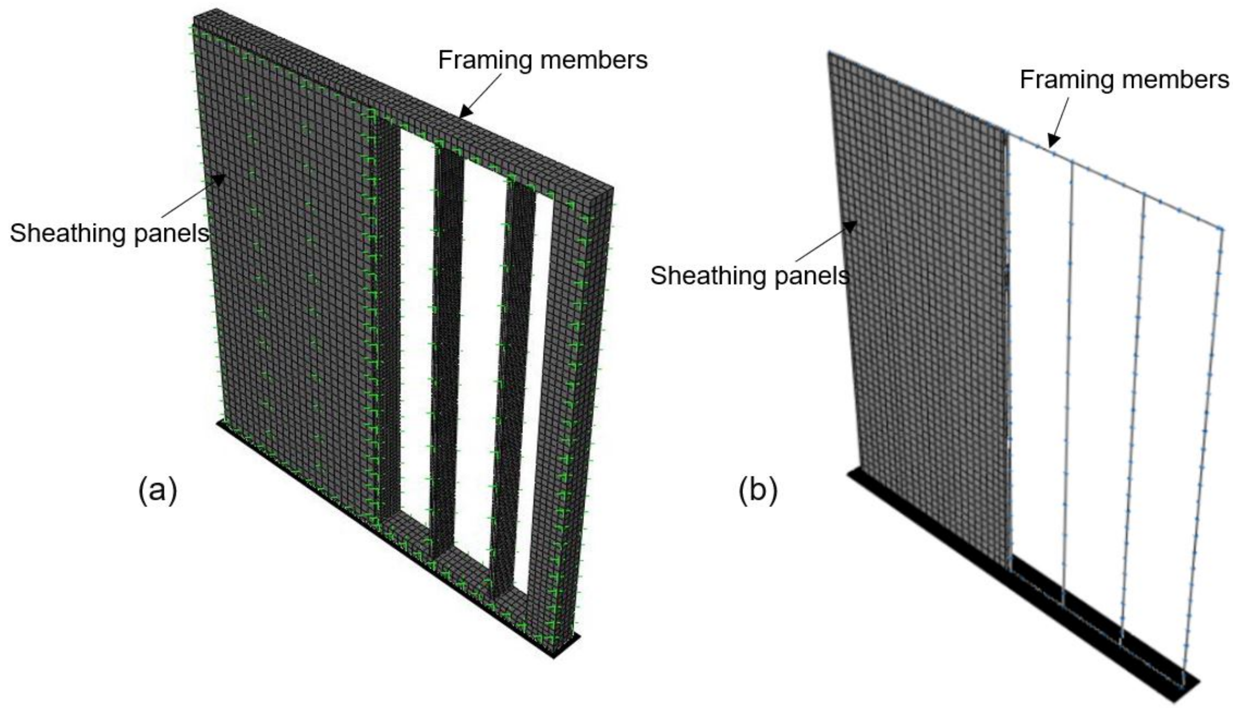

Figure 9: Element types used in the wood light-frame shear wall models:(a) Solid elements model, (b) Beam and shell elements model.

In the 3D solid elements model, all components were represented using solid elements (C3D8R), defined as an 8-node linear brick with three degrees of freedom per node (displacements in the X, Y, and Z directions), with reduced integration and hourglass control. In the beam and shell element model, the stud, foundation, top and bottom plates were modeled using first-order, three-dimensional beam elements (B31), which are isotropic and defined defined by 2 nodes with six degrees of freedom at each node (translations in the x, y, and z directions, and rotations about the x, y, and z directions). The sheathing panels were modeled using 3D shell elements (S4R), which are 4-node elements with six degrees of freedom at each node, quadrilateral, stress/displacement shell elements with reduced integration and a large-strain formulation.

3.5 Sheathing-to-framing connections

The nonlinear behavior of wood light-frame walls is primarily influenced by the force-deformation characteristics of the connections between the sheathing and framing. Therefore, to ensure accurate modeling, the sheathing-to-framing connections were modeled and validated separately using connection test result [3, 47]. Researchers at the University of the Bío-Bío in Concepción, Chile, conducted tests on double shear OSB-radiate pine framing joint specimens using 70-mm-long spiral nails with a shank diameter of 3.0 mm. Figure 10 depicts the experimental setup and presents the monotonic and cyclic outcomes for one specimen. In each monotonic test, both parallel and perpendicular directions to the framing grain were analyzed, and nail performance was found to be nearly identical. However, all cyclic tests were conducted with nails loaded parallel to the grain. Further details can be found in [47]. For the purposes of this study, we assume that nail performance is similar whether the nails are loaded parallel or perpendicular to the grain.

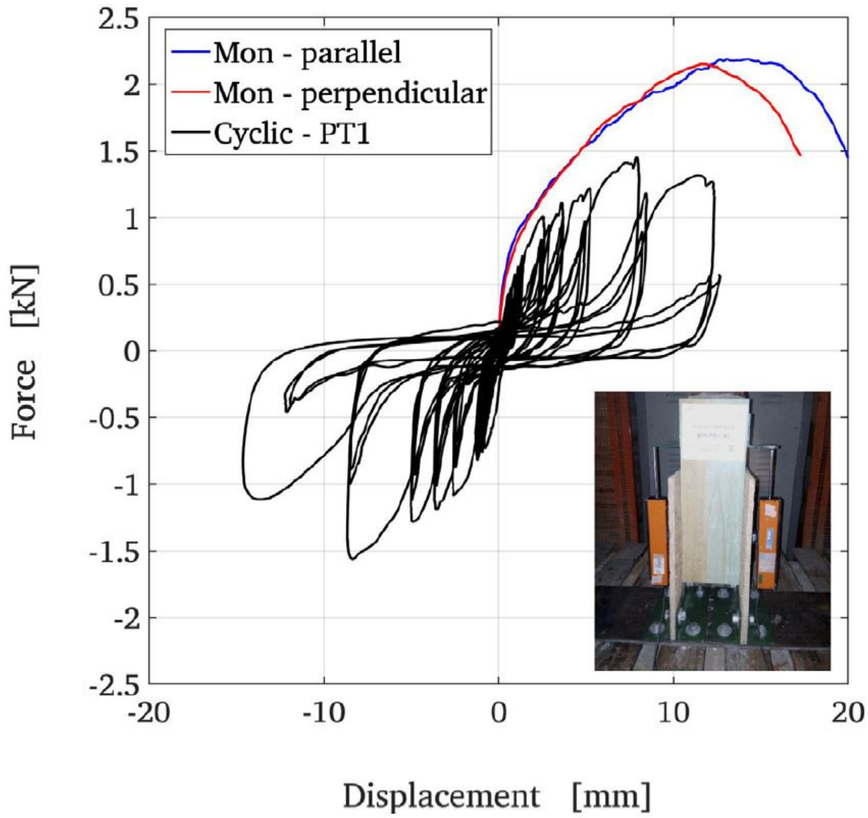

Figure 10: Sheathing-to-framing connection test setup and results under monotonic and cyclic loading. Figure is reproduced with permission from the source [3].

The modified Stewart hysteretic model (MSTEW) proposed by Folz and Filiatrault [36] was adopted in Estrella, et al. [3]. The MSTEW model consists of ten modeling parameters, as shown in Figure 11 and Table 2. Detailed information on the MSTEW model can be found in Folz and Filiatrault [36].

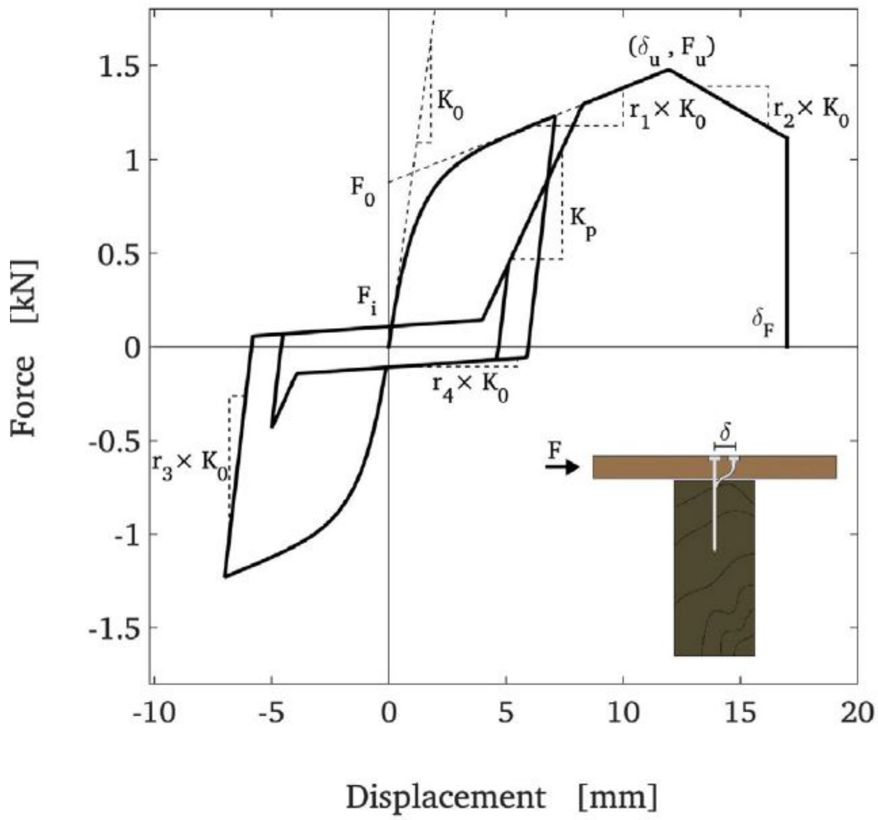

Figure 11: MSTEW model description. Figure is reproduced with permission from the source [3].

Table 2: MSTEW modeling parameters for sheathing-to-framing connections.

Case	**K_0 (kN/mm)**	**r_1**	**r_2**	**r_3**	**r_4**	**F_0 (kN)**	**F_I (kN)**	**δ_u (mm)**	α	β
Estrella, et al. [3]	0.911	0.055	-0.079	1.177	0.010	0.879	0.109	11.951	0.569	1.165
Folz and Filiatrault [36]	0.561	0.061	-0.078	1.400	0.143	0.751	0.141	12.500	0.800	1.100

In this thesis, nonlinear link elements (CONN3D2) used as nail connections incorporate three transitional degrees of freedom. The load-deformation behavior of each connection was characterized by three sets of parameters, as listed in Table 3, covering elastic, plastic, and damage properties. The elastic behavior of the connector is determined by the initial stiffness observed in the connection test responses for the main directions (D11 and D22), which correspond to the X and Y directions, as shown in Figure 13. The third value (D33), representing the stiffness of the connection in the Z direction, constitutes a small percentage of the values in the main directions. The plastic hardening behavior with nonlinear isotropic hardening was defined using tabular data. The isotropic hardening behavior defines the evolution of the yield surface size, F^0 , as a function of the equivalent plastic relative motion, u^{-pl}. This evolution can be introduced by specifying F^0 directly as a function of u^{-pl} in tabular form or by using the simple exponential law [42].

$$F^0 = F|_0 + Q_{inf}\left(1 - e^{-bu^p}\right) \tag{14}$$

where $F|_0$ is the yield value at zero plastic relative motion, and Q_{inf} and b are material parameters. Q_{inf} represents the maximum change in the size of the yield surface, and b defines the rate at which the size of the yield surface changes as plastic deformation develops. When the equivalent force defining the size of the yield surface remains constant $F^0 = Fl_0$, there is no isotropic hardening. Isotropic hardening can be introduced by specifying the equivalent force defining the size of the yield surface, F^0, as a tabular function of the equivalent relative plastic motion, u^{-pl}, and, if required, of the equivalent relative plastic motion rate, u^{-pl}, temperature, and/or other predefined field variables. The yield value at a given state is simply interpolated from this table of data.

Damage behavior was also defined based on relative plastic motion, where linear softening was assumed, as illustrated in Figure 12. If relative motions in a connection exceed critical values, the connector starts undergoing irreversible damage (degradation). Upon additional loading there is further evolution of damage leading to eventual failure. If damage has occurred, the force response in the connector component i will change according to the following general form [42]:

$$F_i = (1 - d_i)F_{\text{eff},i}, \quad 0 \leq d_i \leq 1 \tag{15}$$

where d_i is a scalar damage variable and F_{effi} is the response in the available connector component of relative motion i if damage were not present (effective response). Prior to damage initiation, d has a value of 0.0; thus, the force response in the connector does not change. Once damage has been initiated, the damage variable will monotonically evolve up to the maximum value of 1.0 if damage evolution is specified. Complete failure occurs when d = 1.0.

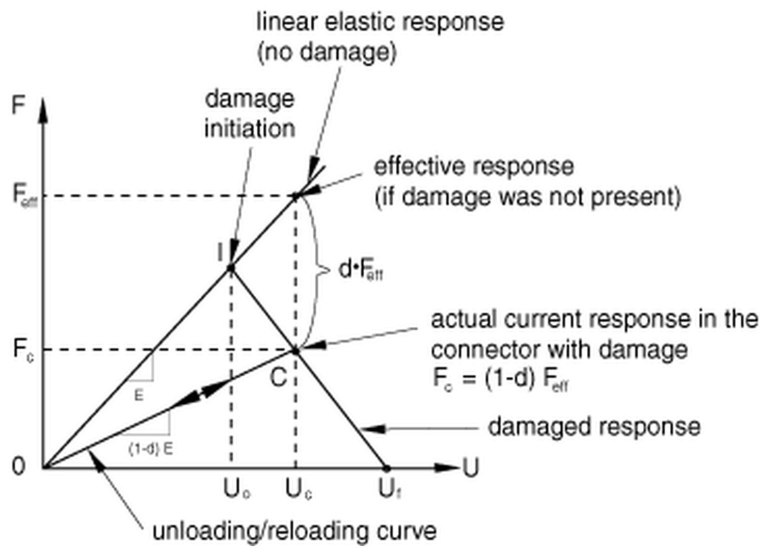

Figure 12: Linear damage evolution law for linear elastic connector behavior. Figure is reproduced with permission from the source [42]

The load-displacement response of the connection model was compared with the average backbone curve of the sheathing-to-framing nail test, as depicted in Figure 13. Overall, the properties employed in the numerical model provide a satisfactory match with the test data. Hence, they can be effectively employed as nail connections in the shear wall model presented in the following section.

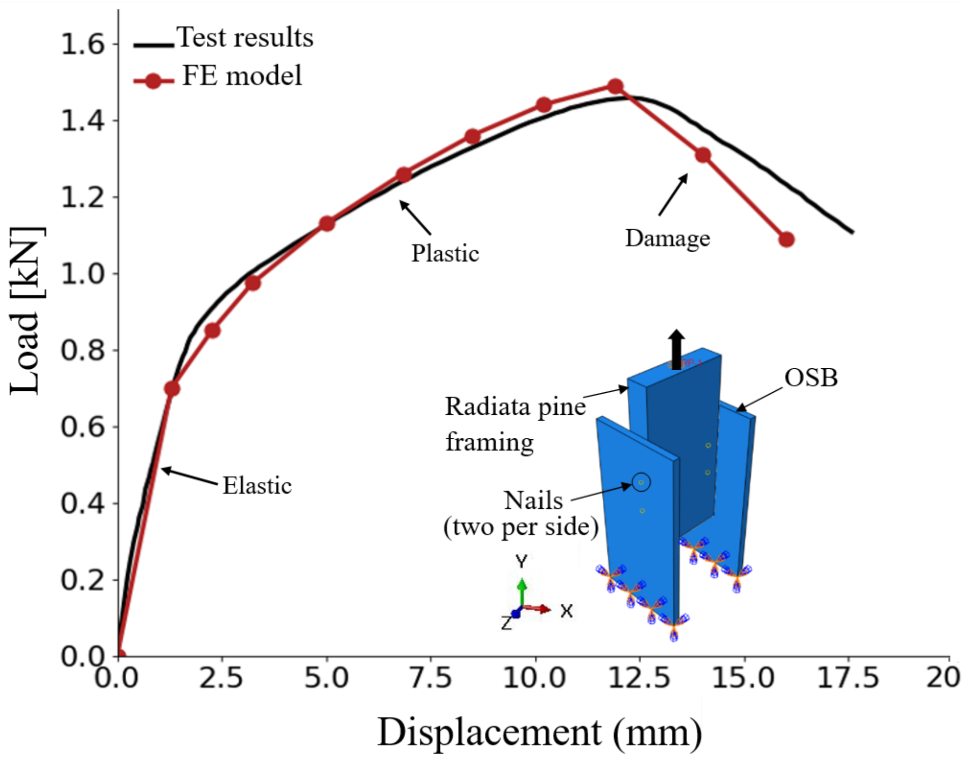

Figure 13: Load-displacement behavior of sheathing-to-framing connection under monotonic loading test, along with an FE model predictions.

Table 3: Sheathing-to-framing connector properties in ABAQUS.

		Elastic Properties			
Property	D11	D22	D33		
Stiffness (N/mm^2)	911	911	12		
		Plastic Properties			
Force (N)	714	879	1040	1290	1470
Displacement (mm)	1.37	2.07	3.78	7.83	11.95
		Damage Properties			
Parameter	Plastic motion at damage initiation		Plastic motion at failure		
Value (mm)	11.95		17		

3.6 Boundary conditions and Loading protocols

In the experiments, the framing elements for the end studs and top and bottom plates were adhered together using high-quality structural glue, ensuring they functioned as a single member even under large deformations. Consequently, in the nonlinear model, these elements were represented as a singular frame element, considering the combined width of all the studs. Following standard practice in wood light-frame construction, only nominal nailing was employed to secure the frame, specifically three 3 $\times$ 100 mm nails per joint in the tested walls. As the contribution of this connection type to the overall stiffness of the wall is small, its effect can be neglected [4, 36]. Thus, framing-to-framing connections (framing nails) were depicted as Tie connections (with free rotations). Sheathing-to-framing connectors (edge and field nails) were modeled using nonlinear link elements, as elaborated in the previous section.

The response of the hold-down system is the result of a complex combination among the wooden members, steel bolts, and anchorage bar. Thus, it is a common practice to depict the load deformation response of hold-downs using a nonlinear hysteretic model that captures their overall behavior. However, when employing high-capacity hold-down, it is reasonable to expect their response to fall within the linear range. As demonstrated, the demands on the hold-downs remain well under their maximum tensile capacity [3]. Therefore, a linear link element, with equivalent stiffness of the hold-downs obtained from the design catalog [80], was utilized to represent them. These linear link elements had a tensile stiffness of kt = 11.85 kN/mm and kt = 94.24 kN/mm for discrete hold-downs and continuous rod hold-downs (44 mm diameter), respectively. The schematic of the shear walls are depicted in Figure 14 and Figure 15 for shear walls with discrete hold-downs and continuous rod hold-downs, respectively.

A rigid foundation was added at the base to simulate high compressive of the reaction steel beam in the test. The horizontal degree of freedom of the bottom plate was restrained to prevent wall sliding. Monotonic (pushover) analyses were performed by applying displacement-controlled loads at the top plate, and the analyses were stopped when the model was no longer able to reach convergence.

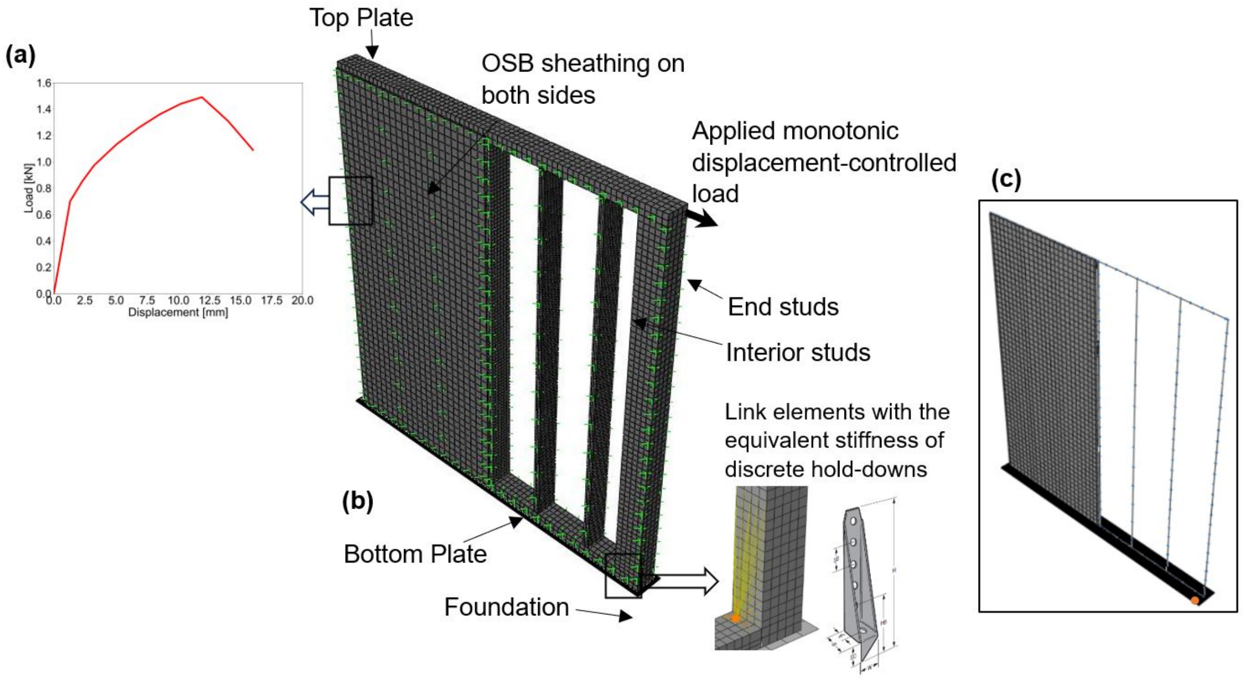

Figure 14: The schematic of the wood light-frame shear wall model with discrete hold-downs: (a) Load-displacement behavior of sheathing-to-framing connectors, (b) 3D view of the finite element model of the shear wall specimen with discrete hold-downs using solid elements, (c) with Beam and shell elements.

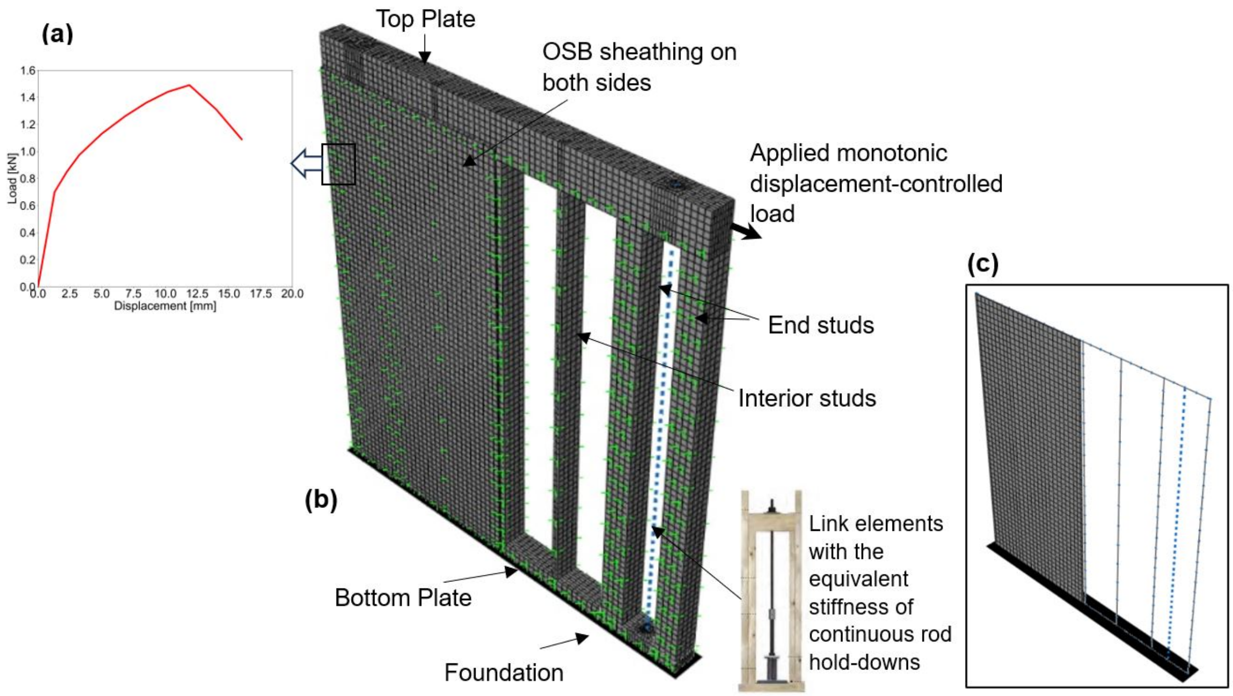

Figure 15: The schematic of the wood light-frame shear wall model with continuous rod hold-down:(a) Load-displacement behavior of sheathing-to-framing connectors, (b) 3D view of the finite element model of the shear wall specimen with continuous rod hold-downs using solid elements, (c) with Beam and shell elements.

3.7 Model validation

Figures 16 show good agreement between the test results and model predictions in terms of initial stiffness, maximum load, and maximum and ultimate displacement. For a detailed assessment of the proposed model, a quantitative comparison between test results and model predictions was also carried out for the shear wall specimens. The initial stiffness is well predicted by the model, with errors of 4.3% and 6.6% compared to average test data for the shear walls with discrete and continuous rod hold downs, respectively. Additionally, the maximum force and maximum displacement are predicted with differences of 1.92% and 4.8%, respectively, for the shear wall specimen with discrete hold downs, and with 3.23% and 8.7%, respectively, for the specimen with continuous rod hold downs.

In addition, analyses showed that the Canadian Standards Association (CSA), and the Special Design Provisions for Wind and Seismic (SDPWS) guidelines as described in section

2.2. slightly overestimate the initial wall stiffness, with the discrepancy increasing at larger displacements. However, CSA O86:19 (section 11.7.1) is more accurate than 2021 SDPWS (Section 4.3.4) equation and captures the nonlinear trend quite well. Nominal shear resistance, provided by standards, represents the theoretical maximum capacity a shear wall can withstand before failure. Considering nominal capacity when comparing deflection values ensures a consistent basis for evaluating performance under design loads. Beyond this point, behaviors like large deflections or failure are less relevant for design.

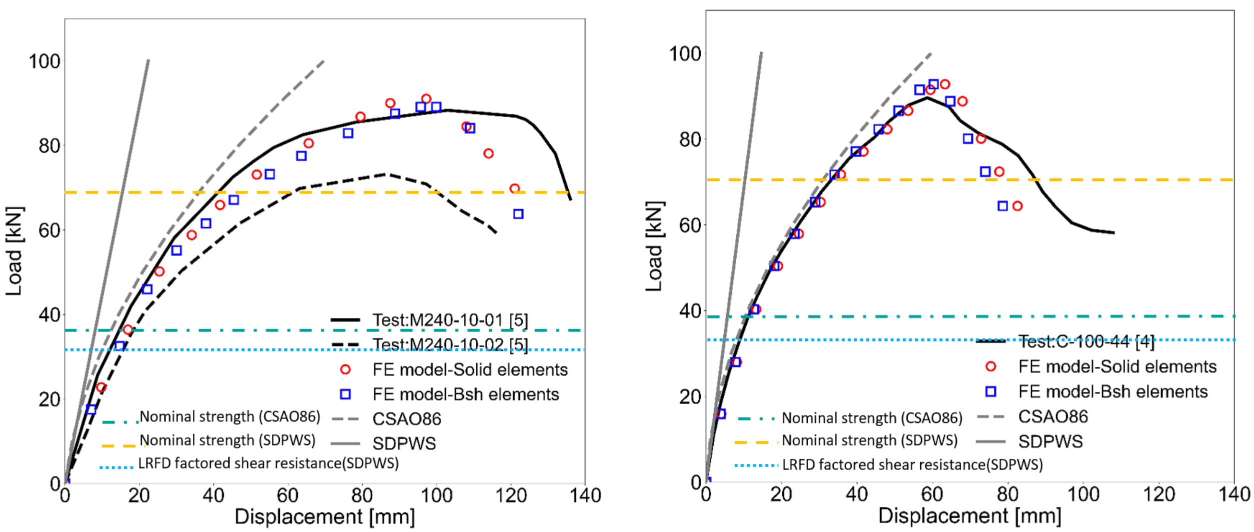

(a) (b)

Figure 16: Comparison of wood light-frame shear wall models with experimental results, and analytical equations: (a) with discrete hold-downs and (b) with continuous rod hold-downs.

The CSA O86:19 (Section 11.6.2) and 2021 SDPWS (Section 4.1.4 and Table 4.3A) guidelines underpredict the resistance. It should be noted that for seismic design per SDPWS, the ASD allowable shear capacity is obtained by dividing the nominal shear capacity by a reduction factor of 2.8, and the LRFD factored shear resistance is determined by multiplying the nominal shear capacity by a resistance factor of 0.5, which is considered here for comparison. For CSA O86, the factored shear resistance is calculated by multiplying the nominal strength by a factor of 0.8. This reduction ensures a consistent safety level across different materials and structural systems. The lines representing these resistances are shown in Figure 16. A range of conventional and strong shear wall specimens with discrete and continuous rod hold-downs was investigated in our previous research [48], confirming these findings. The results for some specimens are provided in Appendix B.

4 Detailed assessment of wall components

This section presents the FE model results and discusses the behavior of strong wood light-frame shear walls, including a detailed investigation of their components under monotonic loading. Three main components of a wood light-framed shear wall include framing members, sheathing panels, and sheathing-to-framing connections as depicted in Figure 17. In wood light-frame walls, the best performance is achieved when most of the energy is absorbed by the sheathing-to-framing connectors through shear deformation, while the framing and the anchorage system maintain their elasticity.

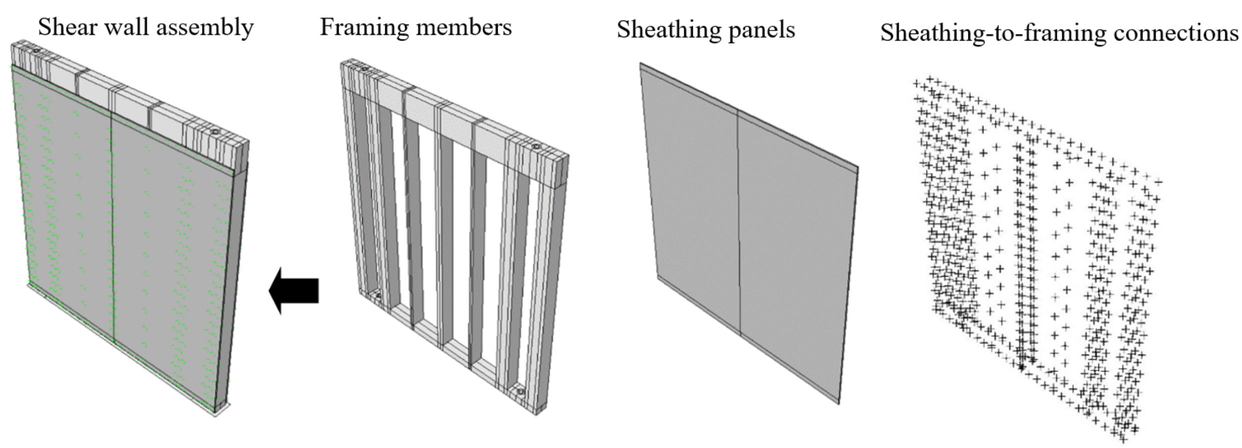

Figure 17: Three main components of a light-frame wood light-frame shear wall: (a) framing members, (b) sheathing panels, and (c) sheathing-to-framing connections.

4.1 Wood components

Wood exhibits complex behavior in different directions (i.e., anisotropic behavior) and under different stress paths. Commonly measured mechanical properties include maximum stress in compression parallel to the grain, compressive stress perpendicular to the grain, and tensile stress perpendicular to the grain, as shown in Table 4 for radiata pine framing [46]. Tensile stress perpendicular to the grain refers to the wood's resistance to forces acting across the grain that tend to split the member. Therefore, it is essential to ensure that the stress distributed in frame members remains below the maximum tensile strength perpendicular to the grain, ensuring that the sheathing-to-framing connections perform well and result in ductile behavior. For sheathing, failure is defined by plane stress criteria as specified by the APA [49]. The in-plane shear and out-of-plane shear strength for a 1200mm wide OSB sheathing panel is provided in Table 4.

Table 4: Mechanical Properties for radiata pine framing and OSB panels [46, 49].

Compression (MPa)		**Tensile (MPa)**	**OSB panels**	
Parallel	**Perpendicular**	**Perpendicular**	**In-plane shear strength (MPa)**	**Out-of-plane shear strength (MPa)**
41.3	5.56	2.78	3.58	3.94

The stress contours of the wood components in the strong wood light-frame shear wall with discrete hold-downs clearly illustrate that the perpendicular-to-grain stress in the end studs significantly exceeds the wood's capacity to withstand such forces. This over stressed condition compromises the structural integrity of the end studs, particularly due to the configuration of the discrete hold-down system, which introduces a risk of crushing the wood under large tensile demands, as shown in Figure 18(a). Additionally, the discrete hold-down system creates stress concentrations at the points where it is bolted to the bottom plate, potentially leading to brittle failure of the frame members (bottom plate), as evidenced by experimental results [5]. The results also reveal that (Figure18) the plane stress in the OSB sheathing panels remains within the structural limits imposed by external forces, suggesting that the OSB sheathing maintains its structural integrity and is less likely to fail under the current loading conditions.

The results indicate that the continuous rod system's configuration helps maintain the structural integrity of the end studs more effectively than discrete hold-down systems. This is because the stress acting perpendicular to the grain of the end studs remains within allowable structural limits, reducing the risk of failure in these critical areas. The robust design of the end studs contributes to additional sheathing-to-framing connections, which enhances the overall stiffness and lateral shear strength of the wall assembly. Consequently, the system shifts the failure mode away from the end studs toward the center of the wall as shown in Figure 19(a), which is more desirable in maintaining structural performance. Additionally, the plane stress in the OSB panels also remains within allowable structural limits, ensuring that the sheathing contributes effectively to the lateral load resistance without experiencing premature failure.

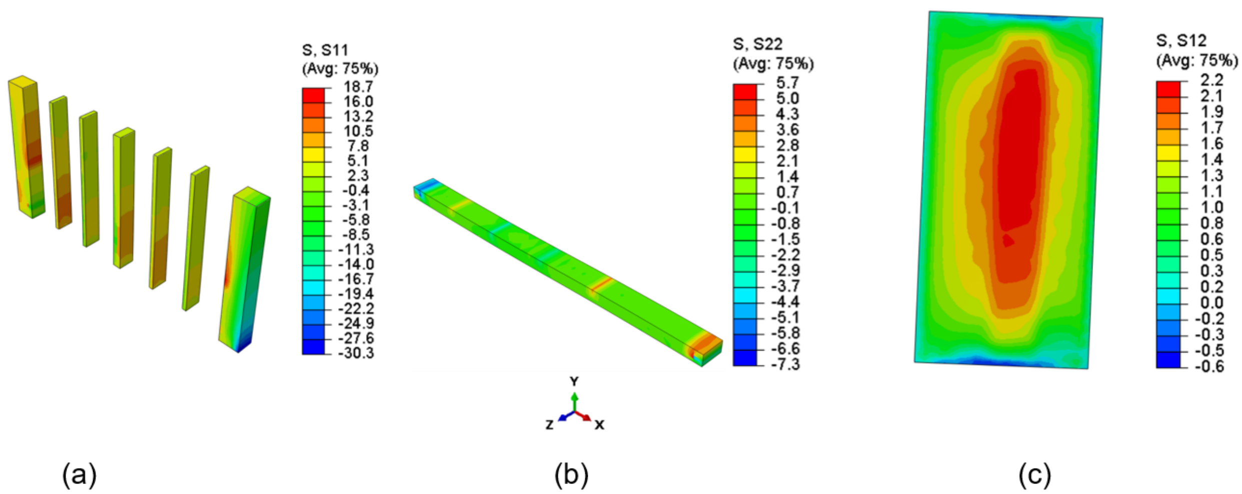

Figure 18: Maximum perpendicular-to-grain stress (in MPa) contours of the strong wood light-frame shear wall with discrete hold-downs, at ultimate displacement (the displacement corresponding to a 20% drop from peak load) (a) studs (Half of the studs are shown due to symmetry.), (b) bottom plate, and (c) plane stress in OSB sheathing panels.

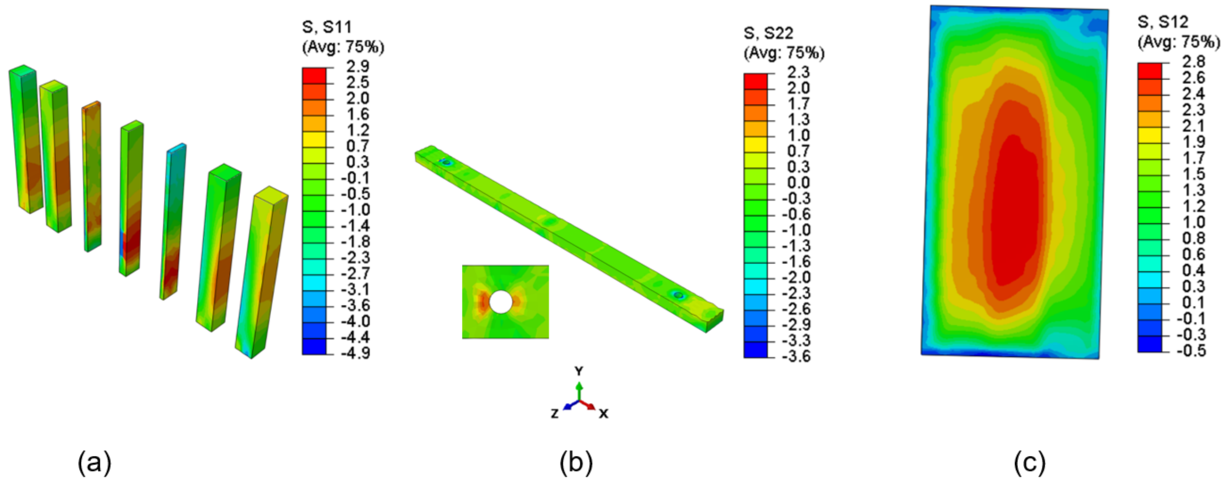

Figure 19: Maximum perpendicular-to-grain stress (in MPa) contours of the strong light-frame wood light-frame shear wall with continuous rod hold-downs, At ultimate displacement (the displacement corresponding to a 20% drop from peak load) (a) studs (Half of the studs are shown due to symmetry.), (b) bottom plate, and (c) plane stress in OSB sheathing panels.

This combination of factors highlights the effectiveness of continuous rod systems in significantly enhancing the overall structural performance, particularly by improving the load distribution and increasing the resistance to lateral forces, making them a reliable solution for maintaining the integrity of shear walls under wind and seismic loading conditions.

4.2 Sheathing-to-framing connections

The deformation of the sheathing-to-framing connections is caused by the relative displacement between the OSB panels (sheathing) and the wood frame. The maximum displacement varies depending on the position of the connection within the wall. Figures 20 and 21 illustrate the maximum displacement contour of the sheathing-to-framing connections and the load-displacement results for several connections in the strong wood light-frame shear walls with discrete hold-downs and continuous rod hold-downs, respectively. The data indicate that connectors at the central studs and at the upper and lower corners experience the greatest deformations and contribute significantly to the wall's overall resistance. For the shear wall with discrete hold-downs, the nail connectors at the end studs undergo plastic deformations and damage, while for the wall with continuous rod hold-downs, the nails at the end studs remain largely undamaged and elastic. This finding is consistent with the damage observed during testing and reported by Estrella et al. [4]. This behavior can be explained by the large number of sheathing-to-framing connections at the end studs, which provide significant redundancy in the nails and increase the shear stiffness in this area. The nail connections positioned at the interior studs contribute minimally to the wall's overall response, primarily serving to prevent the out-of-plane buckling of the OSB panels. Furthermore, Figure 22 shows that even at small lateral displacements (5-15 mm), the nails at central studs in the walls are highly loaded in shear and exhibit a nonlinear response.

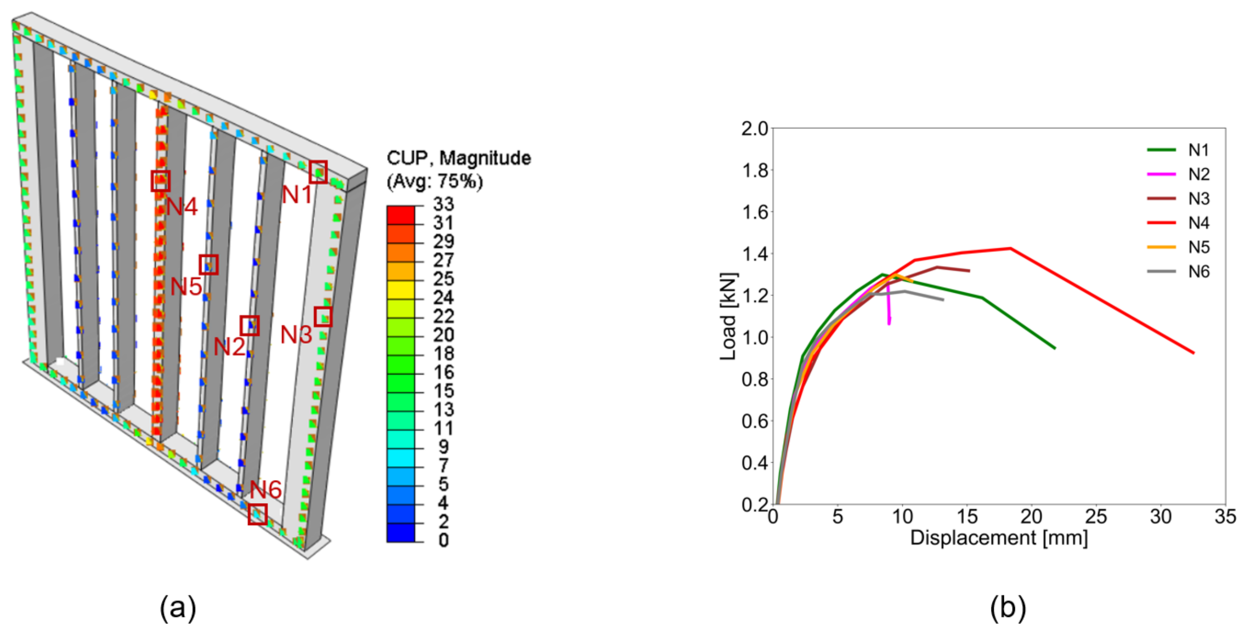

Figure 20: Demands on sheathing-to-framing connections of the strong wood light-frame shear wall with discrete hold- downs, at ultimate displacement (the displacement corresponding to a 20% drop from peak load): (a) displacement contours, (b) load-displacement curves for some connections in the shear wall.

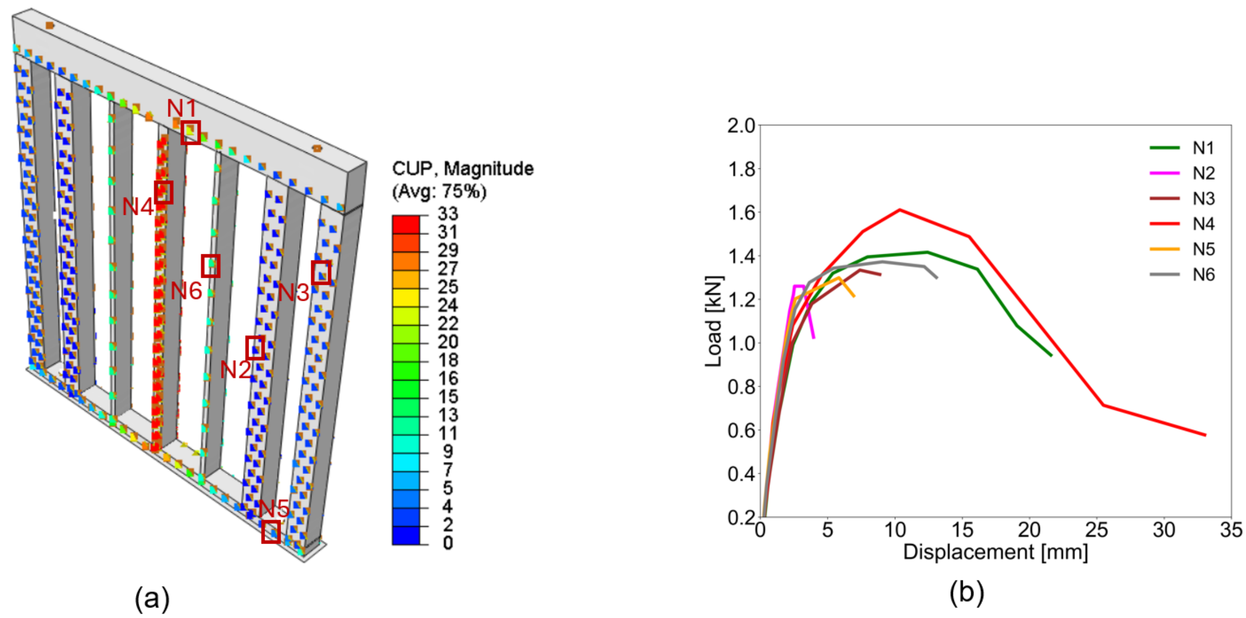

Figure 21: Demands on sheathing-to-framing connections of the strong wood light-frame shear wall with continuous rod hold- downs, at ultimate displacement (the displacement corresponding to a 20% drop from peak load): (a) displacement contours, (b) load-displacement curves for some connections in the shear wall.

The energy dissipated by the sheathing-to-framing connections can be estimated using the Equivalent Energy Elastic–Plastic (EEEP) method, following the guidelines of the ASTM E2126 standard [25]. The load-displacement curves obtained for all sheathing-to-framing connections were idealized as perfectly elastic-plastic curves, with an area equal to that enclosed by the original load-displacement curve, as illustrated in Figure 23 for one of the connections. The initial stiffness is defined as the slope of a line connecting the origin of the coordinate system to a point corresponding to 40% of the peak load. The elastic portion of the bilinear curve is determined by the initial stiffness, while the plastic portion is represented by a horizontal line at the yield point, extending to the ultimate displacement, which corresponds to 80% of the peak load (post-peak). The yield point is calculated by equating the area under the load-displacement curve with the area under the EEEP curve.

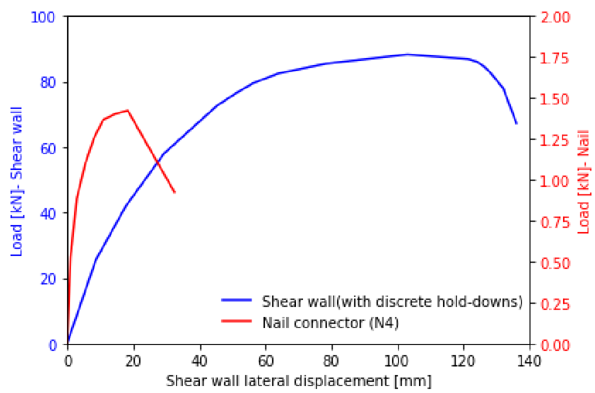

(a)

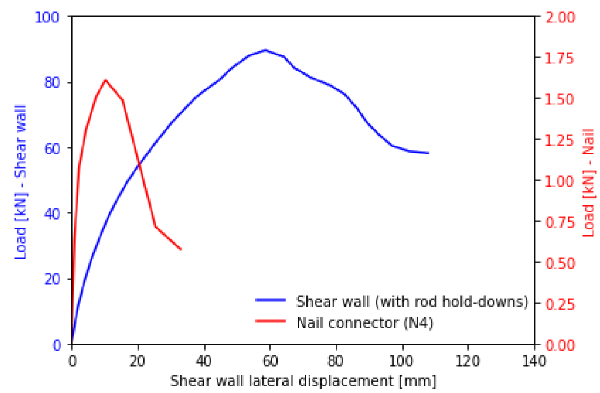

(b)

Figure 22: Load-displacement response of the shear wall, and a nail at the middle section of the wall: (a) with discrete hold-downs and (b) with continuous rod hold-downs.

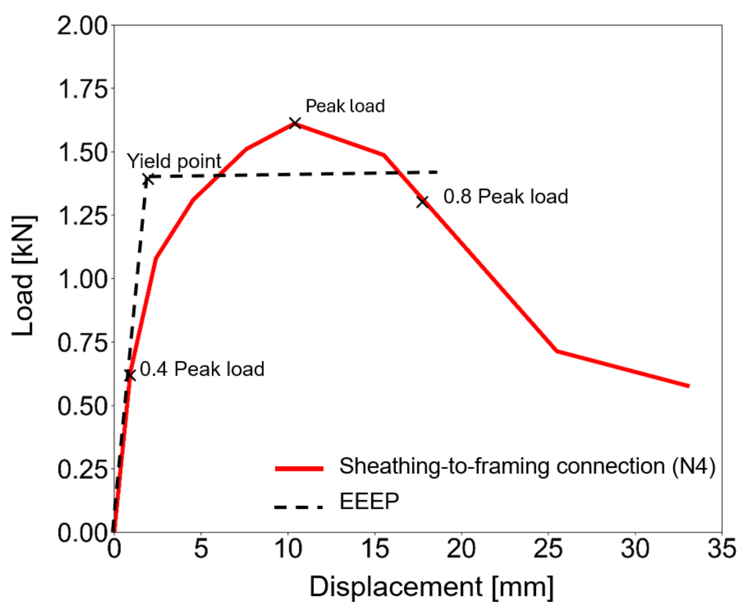

Figure 23: EEEP approach for sheathing-to- framing connection.

Results indicate that the connections at the central studs and corners dissipate more energy and contribute more to the overall deformation of the shear wall. The total energy dissipated by all sheathing-to-framing connections was calculated to be 3635.8 kN-mm for shear walls with discrete hold-downs and 4847.7 kN-mm for those with continuous rod hold-downs. The higher energy dissipation in walls with continuous rod hold-downs suggests enhanced ductility, as these connections can absorb more energy before failure, thus improving the wall's ability to resist seismic or wind loads.

5 Parametric Studies

To assess the influence of various construction detail modifications on shear wall behavior, a comprehensive investigation was conducted on a total of 10 strong shear wall specimens. The study focused on key structural factors, including the perpendicular-to-grain stress in frame members, in-plane stress within oriented strand board (OSB) panels, and the energy dissipation occurring at the sheathing-to-framing connections. These factors play a critical role in determining the overall performance, stability, and durability of shear walls under lateral loading conditions, such as those encountered during seismic events. Table 5 provides detailed information on the wall labels and corresponding milestones associated with each specimen. Notably, the shear wall previously validated in earlier experiments (SW-A) was utilized as the reference specimen for comparison, serving as a benchmark to evaluate the relative performance of the modified designs.

Table 5: Labeling and milestone of the strong wood light-frame shear wall specimens with continuous rod hold-downs.

Wall label	**Milestone**
SW-A	Reference wall
SW-B	Effect of nail spacing
SW-C	Effect of rows of nails (two rows of nails)
SW-D1	Effect of rod diameter (12.7 mm)
SW-D2	Effect of rod diameter (31.7 mm)
SW-E	Effect of adding more inner studs (Close to the current ones)
SW-F1	Effect of OSB panel thickness (12.5 mm)
SW-F2	Effect of OSB panel thickness (15.5 mm)
SW-G	Effect of removing one OSB Panel
SW-H	Effect of modulus of elasticity of OSB sheathing (20% increase)

5.1 Effect of nail spacing and two rows of nails

The effect of varying nail spacing was examined by analyzing the results from the SW-B wall specimen, which featured edge nailing spaced 50 mm on center and field nailing spaced 100 mm on center. In this configuration, the nail spacing was reduced by half compared to the reference shear wall specimen. Additionally, the SW-C specimen utilized two rows of nails along the edges, spaced at 100 mm, to explore the impact of multiple rows of nails on wall performance as tested in Qiang et al. [17]. Figure 24 presents the load-displacement response of the wall specimens, illustrating that wall strength is significantly influenced by nail spacing and the addition of nail rows, with increases of 86.2% and 76.9%, respectively. The stiffness is also expected to be significantly affected, as the results show a 65% increase. These findings align with previous research [17] indicating that shear walls with two rows of nails exhibit twice the lateral load capacity compared to conventional shear walls. Although reducing nail spacing or adding extra rows of nails significantly improves wall strength and stiffness, but this study reveals a critical drawback. These changes generate excessive perpendicular-to-grain stress in the central studs and in-plane stress in the OSB panels, with stress levels exceeding allowable limits by over double as shown in Figure 25, and Table 6. This leads to a more brittle failure mode of frame members. Therefore, the increase in stress levels within the frame members must be carefully considered when optimizing shear wall designs for strength and stiffness.

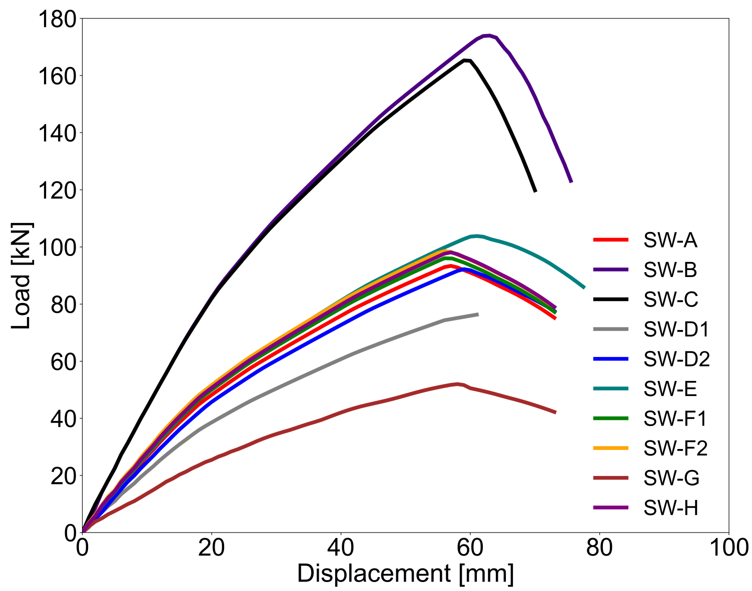

Figure 24: Load-displacement comparison for the walls with different construction details as provided in Table 5.

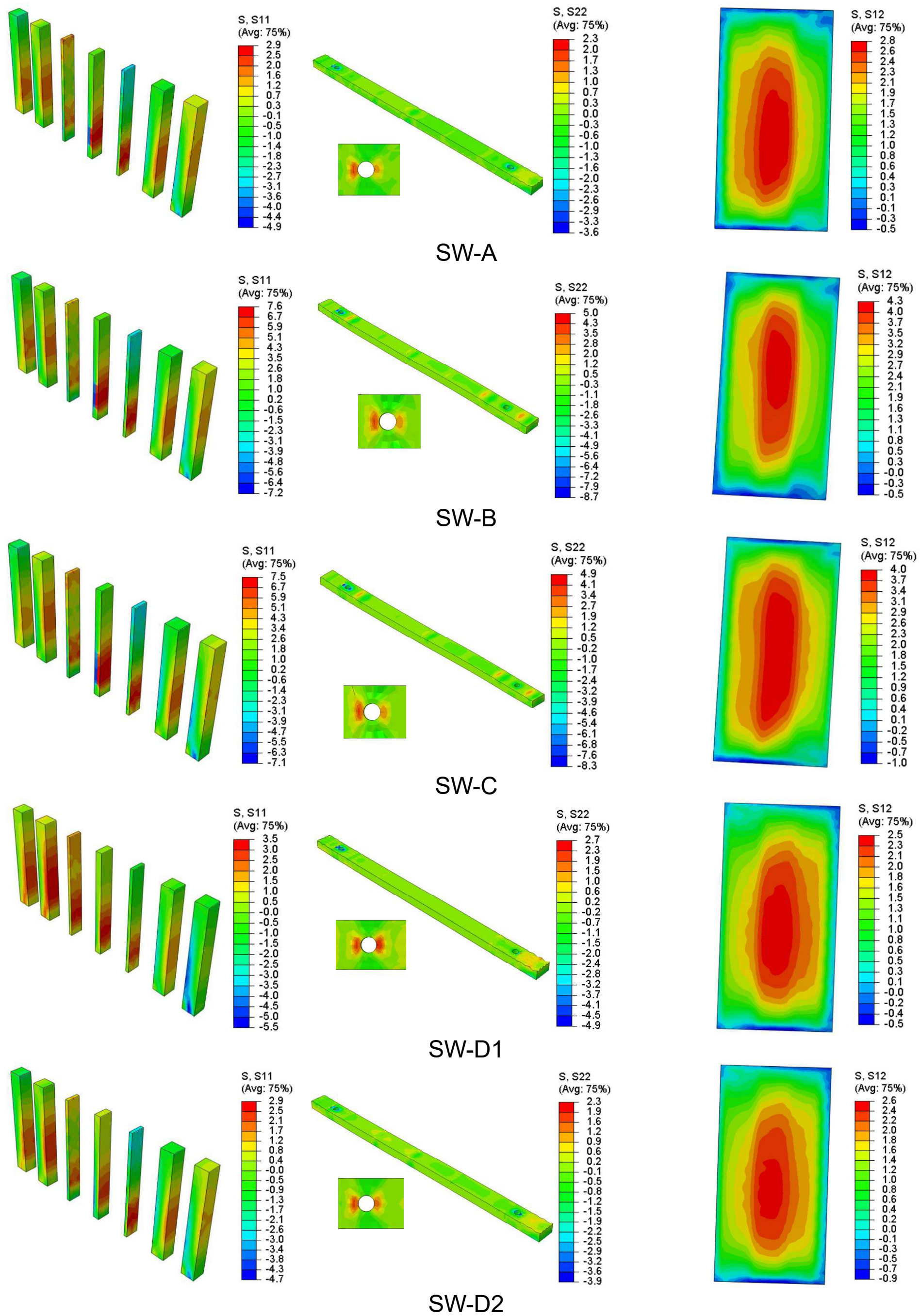
S, S11 (Avg: 75%)
S, S22 (Avg: 75%)
S, S12 (Avg: 75%)
SW-A
S, S11 (Avg: 75%)
S, S22 (Avg: 75%)
S, S12 (Avg: 75%)
SW-B
S, S11 (Avg: 75%)
S, S22 (Avg: 75%)
S, S12 (Avg: 75%)
SW-C
S, S11 (Avg: 75%)
S, S22 (Avg: 75%)
S, S12 (Avg: 75%)
SW-D1
S, S11 (Avg: 75%)
S, S22 (Avg: 75%)
S, S12 (Avg: 75%)
SW-D2

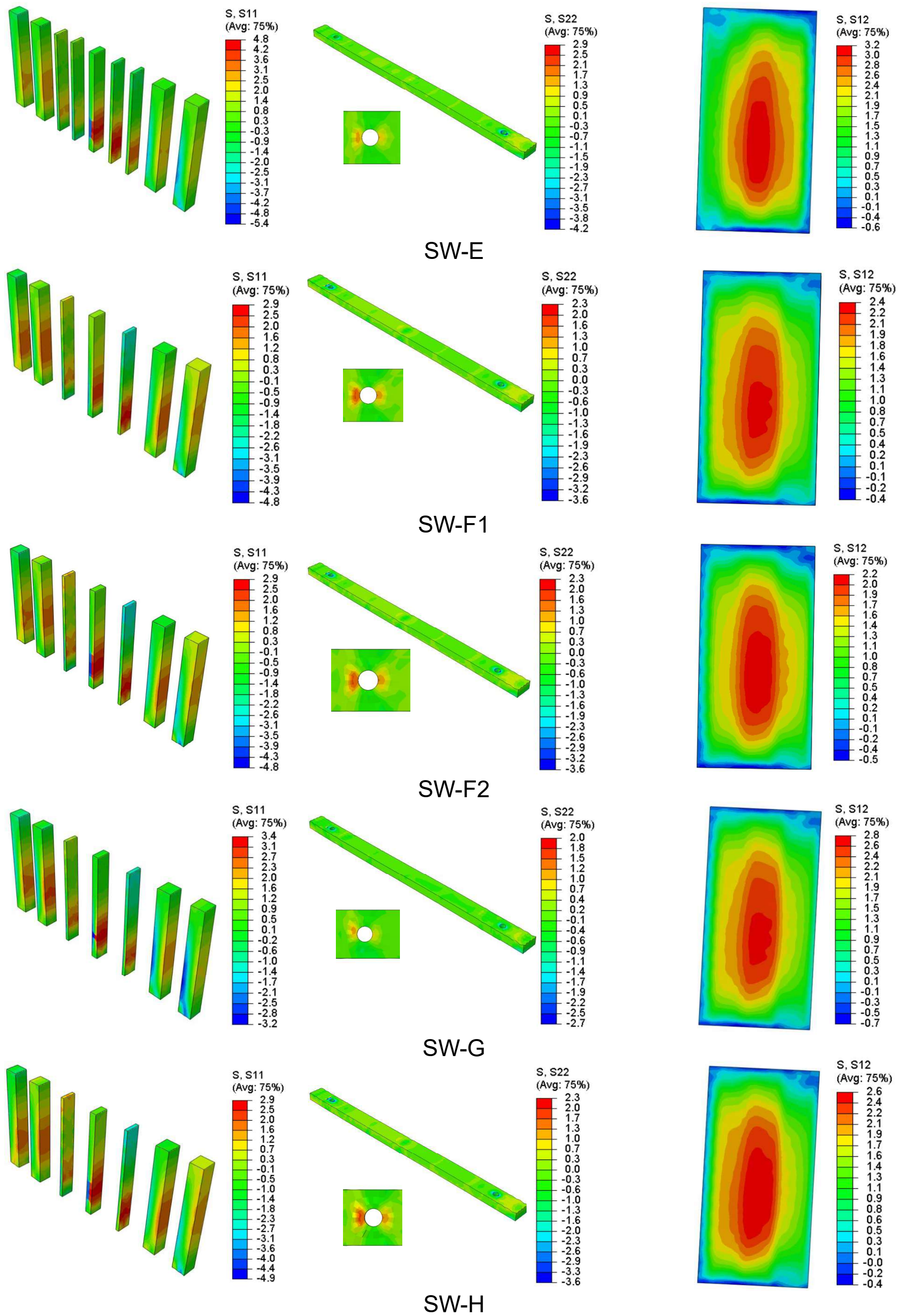

Figure 25: Maximum perpendicular-to-grain stress (in MPa) contours in studs and bottom plates, and plane stress in OSB sheathing panels for the shear wall specimens, at ultimate displacement (the displacement corresponding to a 20% drop from peak load).

Table 6: Summary of the numerical results for each shear wall. The results in other rows are normalized by the values in the first row (control wall) to show the influence of each parameter.

Wall label	Peak load (kN)	Initial stiffness (kN/mm)	Energy dissipated by nails (kN-mm)	Max. perp. to grain stress of studs (MPa)	Max. perp. to grain stress of bottom plate (MPa)	Max. plane stress of OSB sheathings (MPa)
SW-A	**93.4**	**2.6**	**4847.7**	**2.9**	**2.3**	**2.8**
SW-B	1.86	1.65	2.65	2.62	2.17	1.54
SW-C	1.77	1.65	2.34	2.58	2.13	1.43
SW-D1	0.82	0.81	0.45	1.21	1.17	0.89
SW-D2	0.98	0.92	0.89	1.0	1.0	0.93
SW-E	1.11	1.04	1.26	1.65	1.26	1.14
SW-F1	1.03	1.0	1.2	1.0	1.0	0.86
SW-F2	1.05	1.08	1.21	1.0	1.0	0.78
SW-G	0.55	0.5	0.68	1.17	0.87	1.0
SW-H	1.05	1.07	1.22	1.0	1.0	0.93

5.2 Effect of rod hold-down diameter

The effect of continuous rod hold-down diameter was investigated by comparing two wall specimens, SW-D1 and SW-D2, constructed with the same details except for the rod diameters: 12.7 mm for SW-D1 and 31.7 mm for SW-D2. The impact of hold-down diameter on wall strength and stiffness is not very significant, as expected, because the overall behavior of the wall, when any hold-down is present, is generally governed by failure in the sheathing-to-framing connections.

Nevertheless, the use of a stiffer hold-down system (larger diameter) provides important benefits by increasing the wall's overall strength and stiffness, helping to prevent premature failure and minimize rigid body rotation. For example, the 12.7 mm rod hold-down in specimen SW-D1 resulted in non-ductile behavior, as seen in Figure 24, and exhibited the lowest energy dissipation by the nails among all the tested specimens (Table 6). This reduced performance is attributed to the yielding of the smaller rod diameter, which led to the premature failure of the anchorage system. Ideally, the anchorage system should remain in the elastic range to allow the wall to undergo further deformation and fully exploit the nails' shear resistance. Further analysis indicated that, as the smaller anchorage system began to yield, higher stress levels were transferred to the end studs, potentially increasing the risk of splitting (Figuer 25). As summarized in Table 6, the reference specimen (SW-A), which used a larger 44.5 mm rod diameter, exhibited about 10% more energy dissipation through the nails compared to SW-D2, suggesting that although the rod hold-down diameter doesn't have a major influence on the wall's overall strength and stiffness, its role in delaying yielding within the anchorage system is vital. This observation is consistent with the test results reported by Estrella et al. [4], reinforcing the notion that while rod diameter does not dramatically govern wall strength, it plays a secondary role in optimizing nail performance and energy dissipation. Therefore, selecting the correct rod diameter is key to achieving a balance between strength, stiffness, and energy dissipation in shear wall systems.

5.3 Effect of adding more inner studs and removing one OSB panel

The results from the wall with adding inner studs spaced at 300 mm from the existing ones (SW-E) reveal a clear improvement in both wall strength and energy dissipation. However, this enhancement is largely attributed to the increased nail connections rather than the intermediate studs themselves. Notably, the data shows that the maximum perpendicular-to-grain stress in the central studs increased significantly, from 2.9 MPa to 4.8 MPa (Figure 25 and Table 6), exceeding the allowable stress limit and raising the possibility of brittle failure, as can be seen from Figure 25 and Table 6.

The findings also indicate that sheathing the wall on only one side leads to increased bending in the frame, which raises the stress levels in the studs and significantly increases the risk of wood crushing. This uneven stress distribution compromises the structural integrity of the wall, as the studs are forced to bear higher stresses. Furthermore, this configuration caused a 50% reduction in both strength and stiffness compared to a double-sided sheathed shear wall. This substantial decrease in performance highlights the importance of proper sheathing on both sides to ensure adequate load distribution, improved stability, and enhanced overall durability of the structure.

5.4 Effect of OSB panels

Two different panel thicknesses, 12.5 mm and 15.5 mm were investigated in this study (SW-F1 and SW-F2, respectively). The results indicate that the wall with the thicker OSB panel exhibits a slightly higher peak load and initial stiffness. More notably, the specimen with a 12.5 mm OSB panel demonstrated a 21% increase in energy dissipation by the nails compared to the specimen with an 11.1 mm thickness, while the applied stress on the frame remained within the allowable range (Figure 25 and Table 6). This is because the thicker panels prevent edge tear-out of the nails from the sheathing and nail head pull-through caused by the crushing of wood strands in OSB panels, allowing the nails to deform more and eventually withdraw, as shown in Figure 26. For thicker OSB panels (15 mm), nail fracture controls the behavior of the connection. These findings align with experimental results from other studies [3, 6, 8, 47].

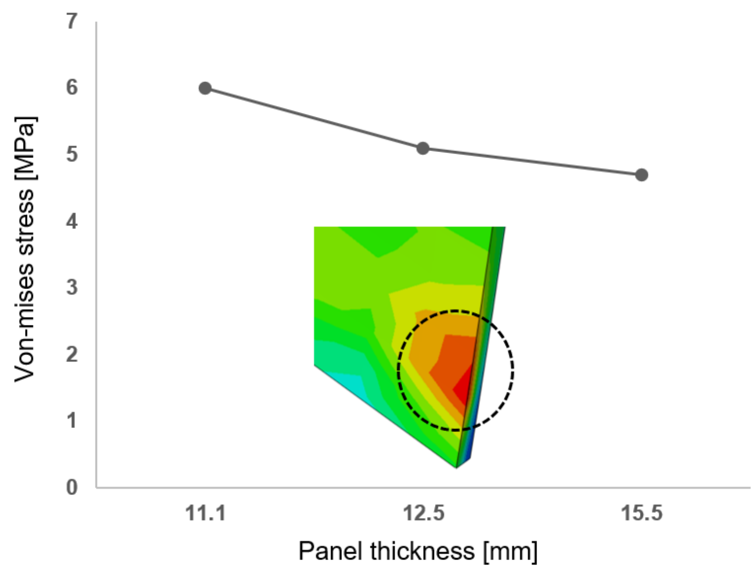

Figure 26: Von-Mises stresses (MPa) in OSB panels near the nail for different panel thicknesses. The nails are spaced at 100 mm, and the distance of the nails from the OSB edge (edge distance) is 18 mm.

Further increasing the OSB panel thickness from 12.5 mm to 15.5 mm has a smaller impact on the wall's strength and energy dissipation, suggesting that there may be an optimal thickness for OSB panels in a shear wall. Moreover, the study found that increasing the modulus of elasticity of the OSB by 20% produced a similar effect on the wall as using the 15.5 mm thick panels, leading to a 22% rise in energy dissipation by the nails. Despite these modifications, the framing and anchorage system remained within the elastic regime. This suggests that panel thickness and material properties are key factors in enhancing the performance of shear walls. Comparing the normalized energy dissipated through the nails and the maximum perpendicular-to-grain stress values of the shear wall specimens with the reference specimen (SW-A), as shown in Figure 27, reveals that the wall specimens SW-F1, SW-F2, and SW-H, which feature thicker OSB panels and panels with higher modulus of elasticity, consistently dissipate more energy through the nails while maintaining the stress on the frame members within the elastic range.

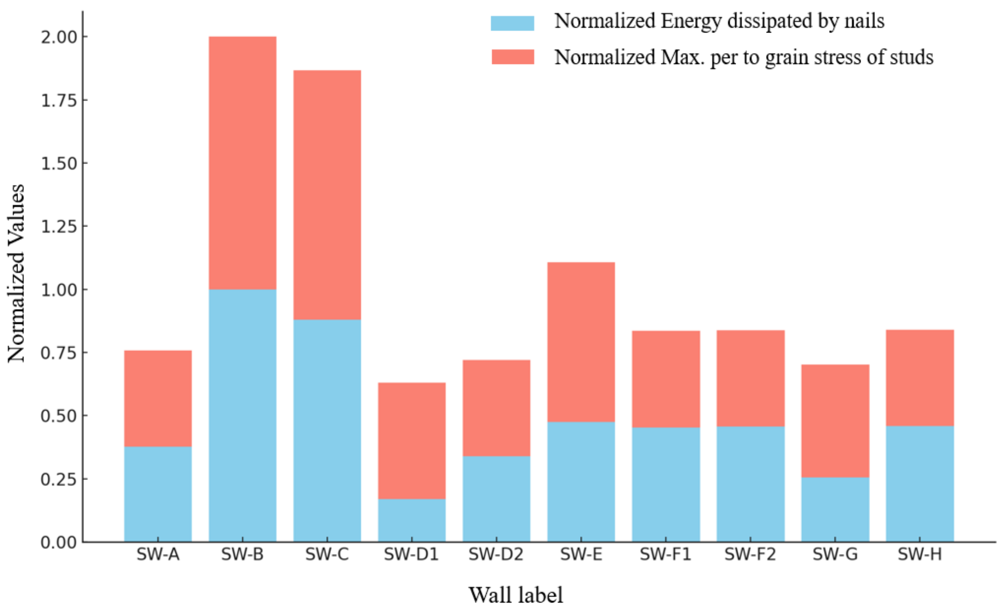

Figure 27: Energy dissipated by the nails and the maximum perpendicular-to-grain stress of studs (normalized to their respective maximum values) for the shear wall specimens.

This suggests that optimizing panel thickness and its mechanical properties can enhance shear wall performance while reducing the need for additional nails. This approach balances the improvement of both strength and ductility in the design of more resilient shear walls. In this context, Malek et al. [50] developed analytical equations to estimate the effective orthotropic properties of a unit cell in strand-based composites, based on their constituent phase properties and microstructural features such as resin thickness, void content, and strand geometry. The accuracy of these analytical predictions was validated by comparing them with numerical results.

6 Cyclic Analysis

Research on the cyclic response of strong wood light-frame shear walls is limited in the published literature due to its complexity. In this study, cyclic analyses were performed using ABAQUS software to validate the model's accuracy under reversed loading paths and to investigate the effect of sheathing-to-framing connector behavior on the overall cyclic response.

The findings of this study, along with other research on the cyclic analysis of wood light-frame shear walls, clearly indicate that only beam and shell elements are appropriate for modeling cyclic behavior. The studs, foundation, top and bottom plates were modeled using isotropic 3D beam elements (B31), defined by 2 nodes with six degrees of freedom at each node (translations in the x, y, and z directions, and rotations about the x, y, and z directions). The sheathing panels were modeled using 3D shell elements (S4R), which are 4-node elements with six degrees of freedom at each node.

6.1 Sheathing-to-framing connection

To accurately model the cyclic behavior of wood light-frame shear walls, it is essential to accurately represent the hysteretic behavior of nail connectors. Commercially available software, including ABAQUS, lacks elements capable of accurately representing the hysteretic behavior of nailed wood joints. In this section, we use two distinct approaches to characterize nail behavior in cyclic analysis. The first approach utilizes the elastic, plastic, and damage properties of nails as described in the monotonic analysis. The second approach employs a user-defined element that is coupled, nonlinear, and history-dependent, incorporating stiffness and strength degradation as well as pinching effects, as introduced by Xu and Dolan [39].

For the first approach, we employed nonlinear link elements (CONN3D2) that include three translational degrees of freedom. These elements are defined by three sets of parameters addressing elasticity, plasticity, and damage. Details of this methodology are elaborated in the monotonic analysis section (Section 3.5).

ABAQUS software features a unique functionality that enables users to create elements that are not present in the standard ABAQUS element library. This is accomplished through a subroutine known as UEL, which operates identically to the existing elements in ABAQUS/Standard. Xu and Dolan [39] developed a nonlinear hysteretic nail connection element using a UEL subroutine in Compaq Visual Fortran, based on the modified BWBN model [38] capable of simulating various hysteresis behaviors. The foundation of this model is the mass-normalized equation of motion (Equation 15) for a single-degree-of-freedom (SDF) system. This system consists of a mass connected in parallel to a viscous damper, a linear spring, and a nonlinear hysteretic spring, as illustrated in Figure 28.

$$\ddot{u}(t) + 2 \times \xi_0 \times \omega \times \dot{u}(t) + \alpha \times \omega^2 \times u(t) + (1-\alpha) \times \omega^2 \times z(t) = f(t) \tag{16}$$

where u = relative displacement of the mass to the base; ξ_0 = linear viscous damping ratio, which equals $\frac{c}{2 \times m \times \omega}$, where c = linear viscous damping coefficient; $f(t) = \frac{F(t)}{m}$; ω = pseudonatural frequency of the nonlinear system; and ω^2 = mass-normalized stiffness; and α = rigidity ratio, which determines the ratio of the final asymptote tangent stiffness to the initial stiffness.

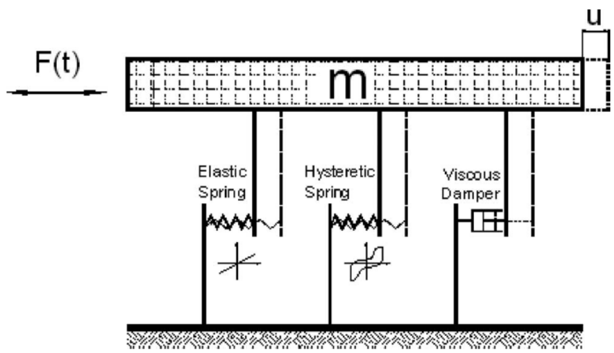

Figure 28: Schematic model. Figure is reproduced with permission from the source [39].]

With modifications by Foliente [51] , the hysteretic displacement is expressed using a differential equation. Additional modifications were introduced by Xu and Dolan [39] to the model, involving adjustments to key parameters and enhancements aimed at resolving various issues in the original formulation. The model requires the identification of 13 parameters. To improve the clarity of the model, Table 7 lists the relevant parameters and their influence on the hysteretic shape. For instance, the parameter n determines the sharpness of the transition from the initial slope to the asymptotic slope during loading (Figure 29). Furthermore, the effect of α is shown in Figure 30. More details about the parameters and their physical meanings can be found in [39, 52]. Foliente [51] provided a suitable set of values for wood nail connectors, determined through repeated trials and comparison with experimental data. However, there are many types of nailed wood joints that may exhibit significantly different performance.

Table 7: Parameters of the model developed by Xu and Dolan [39]

Parameter	**Unit**	**Influence on the hysteretic shape**
p	mm^{-1}	Determines the developing rate of z_1, the pinching stiffness factor, with M_Dis, the maximum experienced displacement.
q	None	Determines the peak pinching location and effects the residual force.
a_0	None	Determines the ratio of the final asymptote tangent stiffness to the initial stiffness.
b	$\text{mm}^{1/n}$	Act as a couple and determine whether the curve is hardening or softening, also affects the ultimate hysteretic spring force.
g	$\text{mm}^{1/n}$	Act as a couple with the b parameter
w	$(\text{kN/mm})^{1/2}$	Determines the initial stiffness of the system.
z_{10}	None	Basic value of z_1, the pinching stiffness factor.
n	None	Determines the sharpness of the transition from initial slope to the slope of the asymptote.
y_0	$\text{mm}^{2/3}$	Basic value of z_2, the pinching range factor.
d_y	$\text{mm}^{-1/3}$	Determines the developing rate of z_2, the pinching range factor, with M_Dis, the maximum experienced displacement.
d_n	$(\text{kN·mm})^{-1}$	Determines the strength degradation rate.
x_0	$(\text{kN·mm})^{1/2}/\text{s}$	The linear viscous damping ratio.
d_h	$(\text{kN·mm})^{-1}$	Determines the stiffness degradation rate.

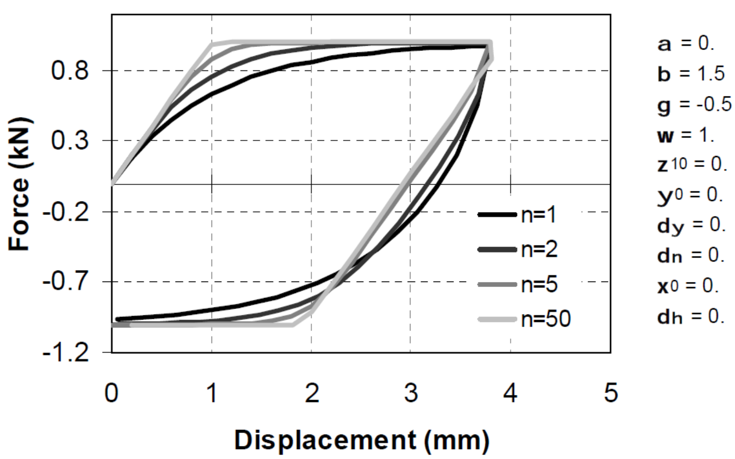

Figure 29: Effect of n on the Shape of the Hysteretic Curve. Figure is reproduced with permission from the source [52]

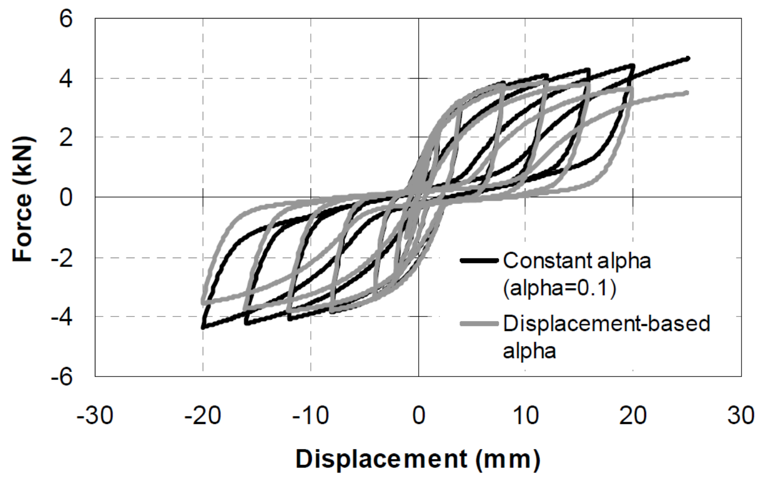

Figure 30: Effect of α on the Shape of the Hysteretic Curve. Figure is reproduced with permission from the source [52]

To demonstrate the effect of the parameters on the model's output visually, connections with 3 different sets of parameters were considered by varying a_0, w, and the combination of a_0 and w, while other 11 parameters are assumed constant. The assumed constant values are provided in Figure 31 . The results (Figure 31) of these models show that each parameter influences the hysteretic shape in to some extent. When two parameters are changed simultaneously, the resulting shapes of the specimens differ from those of the individual parameters, indicating some interaction of the parameters.

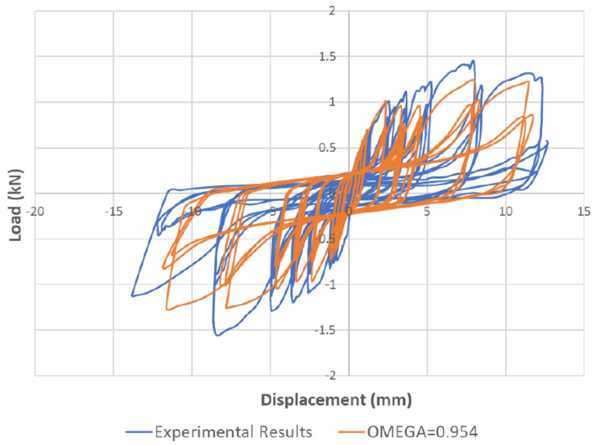

(a)

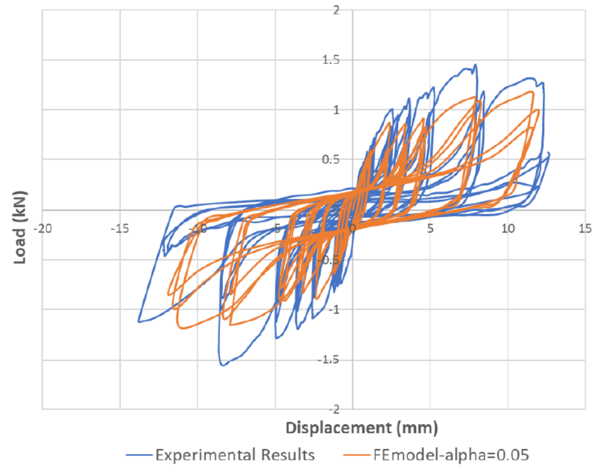

(b)

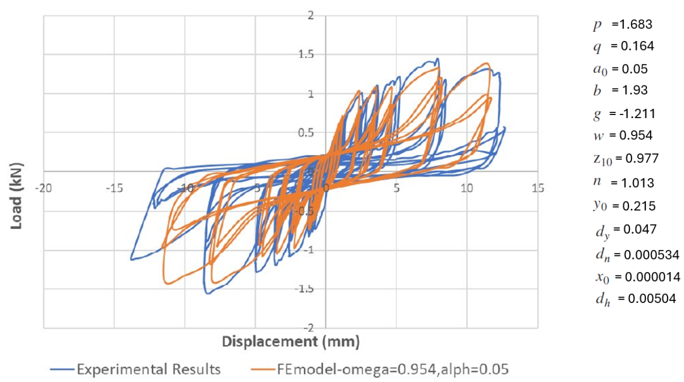

(c)

Figure 31: Hysteresis shape of the FE model versus experimental results. (a) omega=0.954, (b)alpha=0.05, and (c) omega=0.954 and alpha= 0.05

Determining the optimal estimation of each parameter for every nail connection is a complex task. Suitable parameters for different joint configurations can be estimated using genetic algorithms as described in Xu and Dolan [39]. In this study, a set of parameters was selected through a trial-and-error approach to achieve the closest match to the experimental data. The cyclic responses for the sheathing-to-framing connection models using UEL elements and connectors with damage parameters are shown in Figure 32 and were subsequently used for full shear wall modeling.

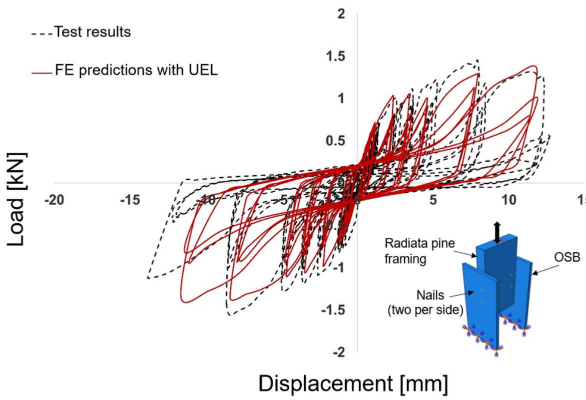

(a)

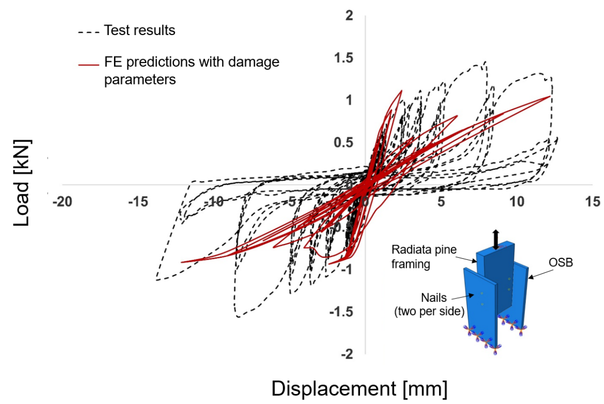

(b)

Figure 32: Load-displacement behavior of sheathing-to-framing connection under cyclic loading test, along with an FE predictions: (a) Using the hysteretic UEL elements (Input parameters of Figure 31(c)) and (b) Using connectors with damage properties (Input parameters of Table 3).

6.2 Boundary conditions and Loading protocols

The boundary conditions used in the cyclic analysis are the same as those in the monotonic analysis described in section1.5.2, except for one approach in modeling sheathing-to-framing connections and the loading protocols. The sheathing-to-framing connections were modeled as outlined in the previous section. The schematic of the shear walls are depicted in Figure 33 and Figure 34 for shear walls with discrete hold-downs and continuous rod hold-downs, respectively.

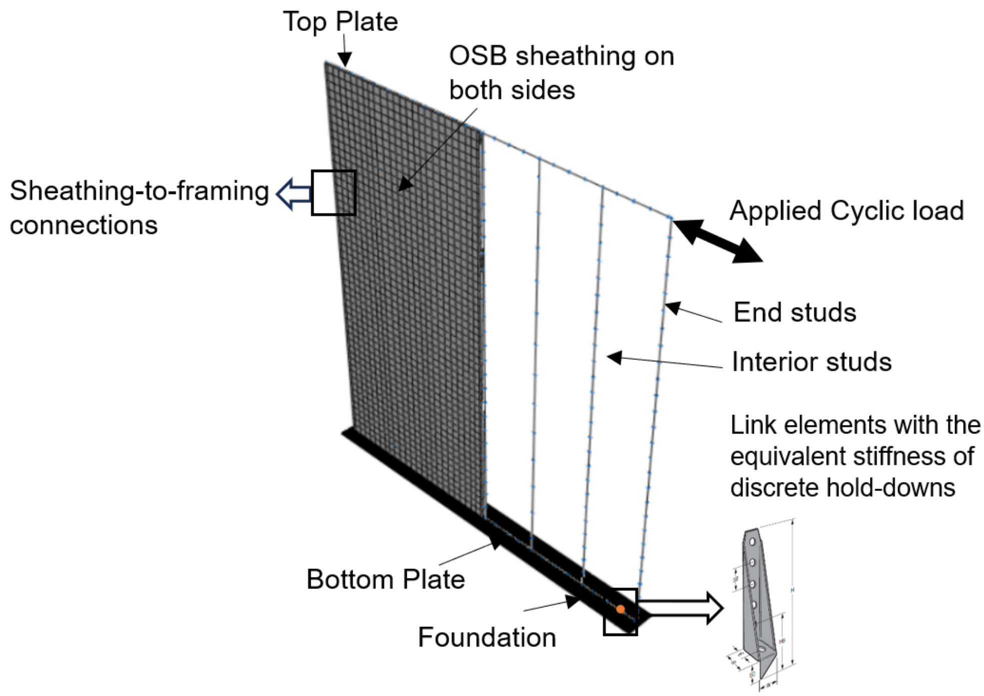

Figure 33: Schematic of the wood light-frame shear wall with discrete hold-downs model, using beam and shell elements, under cyclic loading.

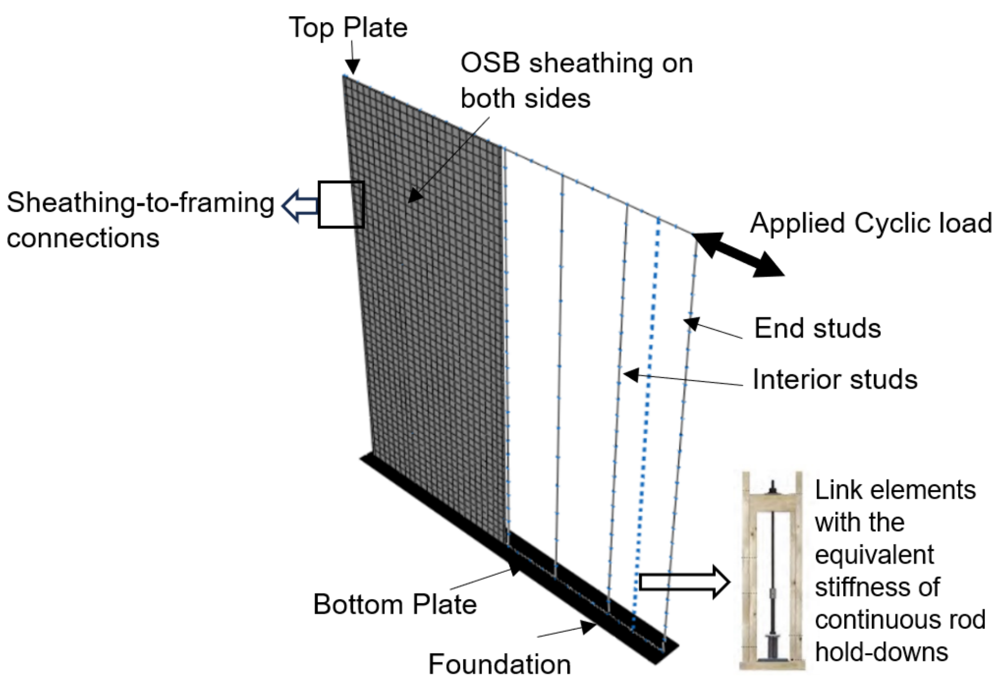

Figure 34: Schematic of the wood light-frame shear wall with continuous rod hold-downs model, using beam and shell elements, under cyclic loading.

The shear walls were subjected to cyclic loading according to the CUREE test protocol proposed by Krawinkler et al. [53]. This protocol was chosen because it allows for the evaluation of the seismic performance of structural elements under conditions similar to those expected during earthquake events with a 10% probability of exceedance over 50 years. As depicted in Figure 35, the loading history comprised various deformation amplitudes, including initiation cycles, primary cycles, and trailing cycles. The reference parameter is the displacement, defined as a fraction of the ultimate displacement obtained from a preliminary monotonic test. The protocol begins with a sequence of six initiation cycles, representing the cumulative damage from minor earthquakes that may have occurred during the specimen's lifetime before the main seismic event. Following these, the primary and trailing cycles are applied alternately. The amplitude of the trailing cycles is 75% of the amplitude of the preceding group of primary cycles. The loading protocol was applied in a displacement-controlled manner.

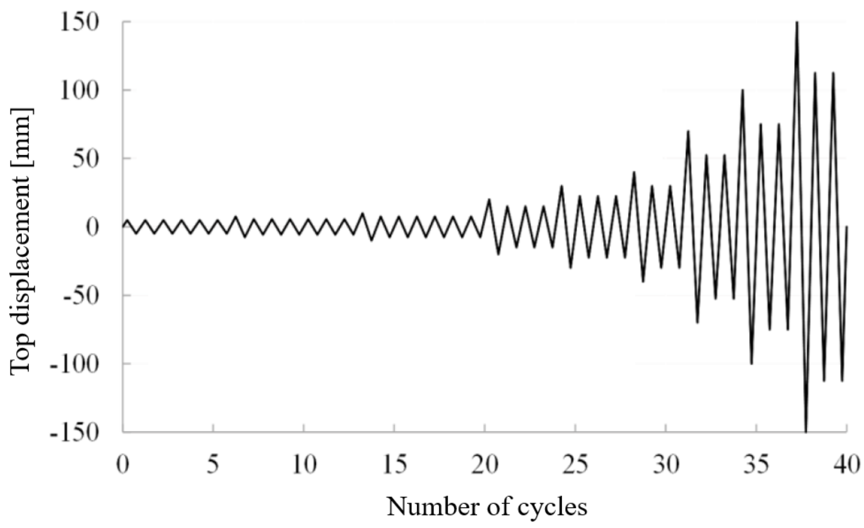

Figure 35: Reversed loading protocol used in cyclic tests.

6.3 Model validation

The hysteresis force–displacement curves from the FE models were compared with the experimental results of the C240-10-01 specimen (with discrete hold-downs) and the C-100-44 specimen (with continuous rod hold-downs)[4, 5], as shown in Figure 36. The FE model, which uses UELelements with nonlinear hysteretic behavior developed by Xu and Dolan [39], shows good agreement with the experimental data, accurately capturing the hysteresis behavior of shear walls. A more detailed comparison between these models and the experimental results, including initial stiffness, maximum force, and total energy dissipated (calculated as the area enclosed by the hysteresis loops throughout the loading protocol), is provided in Table 8. The comparison between the experimental and model results shows that the model with hysteretic UEL elements accurately predicts the maximum force, corresponding displacement, and initial stiffness for both discrete hold-downs (C240-10-01) and continuous rod hold-downs (C-100-44), with differences of up to 10%. However, to accurately capture the force degradation and ultimate displacement, a more precise estimation of the connection parameters is needed. The shear wall results, using elastic, plastic, and damage properties derived from monotonic test data, show discrepancies in capturing the hysteresis loop areas. However, they demonstrate good accuracy in predicting force degradation and ultimate displacement.

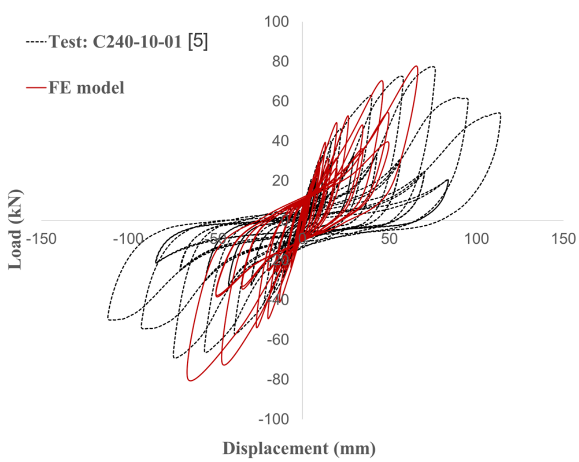

(a)

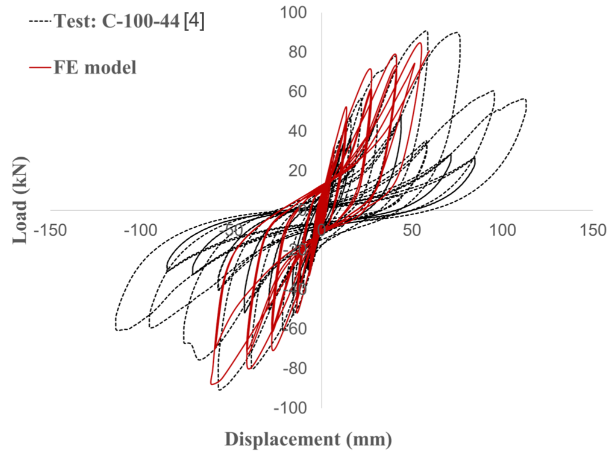

(b)

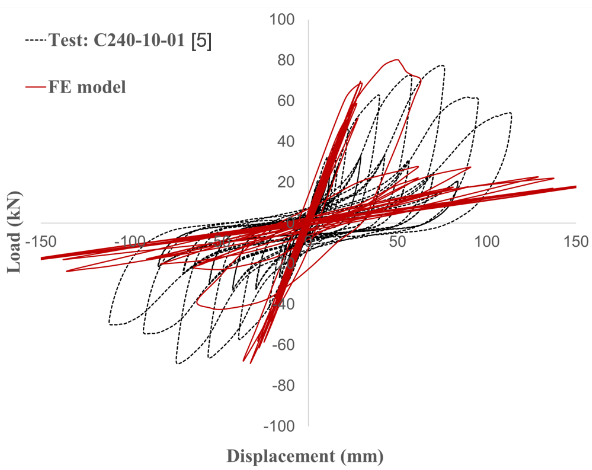

(c)

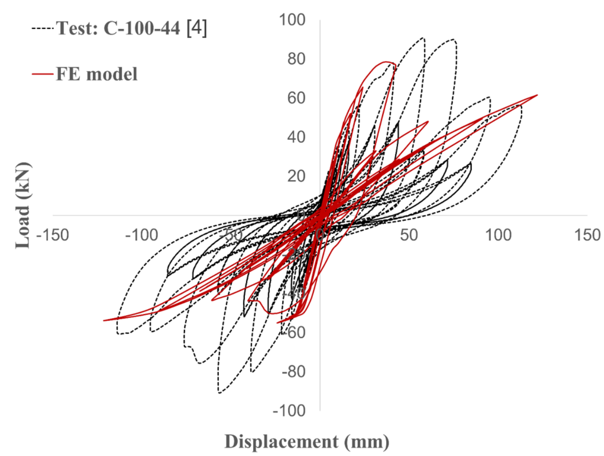

(d)

Figure 36: Comparison of wood light-frame shear wall models under cyclic loading against experimental results: (a) with discrete hold-downs using the hysteretic UEL elements (b) with continuous rod hold-downs using the hysteretic UEL elements (c) with discrete hold-downs using damage properties, and (d) with continuous rod hold-downs using damage properties.

Table 8: Comparison of shear wall model results with experimental data under cyclic loading.

	Stiffness [kN/mm]		Fmax [kN]		Disp. at Fmax [mm]		Energy dissipated [kN · mm]	
	Exp.	**Model**	**Exp.**	**Model**	**Exp.**	**Model**	**Exp.**	**Model**
Discrete hold-downs C240-10-01	2.85	3.02 (6% error)	77.50	77.52 (0.03% error)	75.4	67.5 (10.5% error)	35025.63	19829.86 (43.4% error)
Continuous rod hold-downs C-100-44	6.19	6.59 (6.5% error)	89.67	84.36 (5.9% error)	56.6	54.9 (3% error)	38888.27	22664.32 (41.7% error)

Results demonstrate that the two modelling approaches may be used depending on the main objective of the simulation (capturing peak load, displacement, energy dissipation, or force degradation after reaching its maximum value), and the accuracy level needed. It should be noted that the UEL approach requires the calibration of 13 parameters, which is a tedious process and must be done for each wall configuration. In contrast, the approach using the elastic, plastic, and damage properties of nail connections relies on fewer parameters, making it easier to characterize through small-scale connection tests. In terms of efficiency, the UEL approach requires smaller time steps in ABAQUS using the automatic time-stepping, resulting in computational times that are ten times longer than the other approach. While these approaches demonstrate reliability, their accuracy remains insufficient for comprehensive analysis. To address this limitation, further numerical studies are recommended to gain a deeper understanding of how various input parameters influence the results and to identify the sources of discrepancies between the numerical models and experimental test outcomes. Such investigations could help refine the models and improve their predictive capabilities, bridging the gap between simulations and observed behavior.

7 Conclusions

The behavior of strong wood light-frame shear walls under large lateral loads was investigated using a 3D finite element (FE) model. The study focused on single-story shear wall configurations with both discrete and continuous rod hold-downs under monotonic and cyclic loading, which are validated by comparing the results with experimental data from the literature. The primary objectives were to examine the effects of various parameters on shear wall behavior, evaluate the stresses on the wood components, and assess the energy dissipated by the nails to ensure non-brittle performance. The key conclusions of the study are:

- The FE analysis indicates that discrete hold-down systems can overstress the end studs, compromising their structural integrity and increasing the risk of wood crushing, as demonstrated by experimental work conducted by other researchers [5]. In contrast, continuous rod systems mitigate these risks by maintaining stress levels within allowable limits, thereby enhancing the wall's overall lateral resistance and structural integrity.

- The monotonic results indicate that the connectors at the central studs and corners experience the highest levels of deformation and energy dissipation. In shear walls with discrete hold-downs, the nail connectors at the end studs undergo plastic deformation, hence they are more susceptible to damage. However, in walls with continuous rod hold-downs, the nails at the end studs remain mostly undamaged and elastic, with maximum stress concentrated near the center.

- Nail spacing and the use of multiple rows of nails have the greatest influence on the strength and stiffness of the wall. Reducing the nail spacing by half increased the strength by 86.2%, while incorporating two rows of nails increased the strength by 76.9%. These changes also increased the stiffness by 65%. However, these configurations may lead to significant perpendicular-to-grain stress in the studs and the in-plane stress in the OSB panels that could exceed allowable limits by more than double, leading to crushing of the wood components which is not desirable under seismic events.

- The impact of rod hold-down diameter on wall strength and stiffness was found to be negligible, as shown in other research, since wall behavior is primarily governed by failure at the sheathing-to-framing connections. However, stiffer hold-downs with larger diameters can help prevent crushing of stud and premature failure of the shear wall. The wall with 12.7 mm rod hold-downs exhibits non-ductile behavior due to early yielding of the hold-down, which reduces shear deformation caused by nails and increases stress on the end studs, potentially leading to crushing of the end studs and non-ductile behavior of the wall.

- Removing OSB panels from one side increases bending in the frame, leading to higher stress levels in the studs and a greater risk of wood crushing. This configuration also reduces strength and stiffness by 50% compared to a shear wall with sheathing on both sides. Hence, the use of double-sided shear walls (100% more OSB material compared to one-sided shear wall design) in mid-rise buildings located in high seismic regions is highly recommended, as they provide enhanced lateral strength (44.4%), stiffness (50%), and energy dissipation (32.2%), ensuring better performance and safety during seismic events.

- A shear wall with a thicker OSB panel (12.5 mm) exhibits 21% more energy dissipation through the nails compared to an 11.1 mm panel with identical number of nails, while keeping stress of wood members within their elastic regime. The thicker panels prevent edge tear-out and nail head pull-through caused by the crushing of wood strands in the OSB, allowing the nails to deform more and eventually withdraw. This enables larger deflection and energy dissipation at the nails. Increasing the panel thickness to 15.5 mm has a smaller impact on wall strength and energy dissipation, suggesting an optimal OSB panel thickness. Additionally, a 20% increase in the OSB's modulus of elasticity boosts nail energy dissipation by 22% . Hence, Optimizing panel thickness and mechanical properties enhances shear wall performance while reducing the need for extra nails, balancing improvements in both strength and ductility for more resilient shear walls.

- Accurately modeling the cyclic behavior of shear walls in ABAQUS requires a very detailed calibration assessment of the nonlinear hysteretic behavior of sheathing-to-framing connectors. In this study, a previously calibrated nail model in the literature [39] was implemented via the UEL subroutine to model strong wood light-frame shear walls. While the model successfully predicts maximum force, corresponding displacement, and initial stiffness, more precise estimation of connection parameters is necessary to accurately capture beyond the peak force and energy dissipation. Shear wall models using nail connections with elastic, plastic, and damage properties derived from monotonic test data were shown to have limitations in capturing entire hysteresis loops. However, they demonstrate good accuracy in predicting force degradation and ultimate displacement under cyclic loading. The choice between these two modeling approaches depends on the main objective of the simulation and the required level of accuracy.

- Future studies could focus on experimental testing of walls with different edge distances and spacing of nails as well as thicker OSB panels that have optimized properties to validate the enhanced performance of the shear wall system. Additionally, incorporating damage models in the wood members to improve the cyclic model's accuracy in capturing hysteresis loops could be a valuable area for further research.

References

[1] Canadian Commission on Building and Fire Codes. *National Building Code of Canada*. `https://doi.org/10.4224/w324-hv93`. 2020.

[2] Canadian Commission on Building and Fire Codes. *National Building Code of Canada*. `https://doi.org/10.4224/40002005`. 2015.

[3] Xavier Estrella et al. "Efficient nonlinear modeling of strong wood frame shear walls for mid-rise buildings". In: *Engineering Structures* 215 (2020), p. 110670.

[4] Xavier Estrella et al. "Experimental study of the effects of continuous rod hold-down anchorages on the cyclic response of wood frame shear walls". In: *Engineering Structures* 230 (2021), p. 111641.

[5] Felipe Guíñez, Hernán Santa María, and José Luis Almazán. "Monotonic and cyclic behaviour of wood frame shear walls for mid-height timber buildings". In: *Engineering Structures* 189 (2019), pp. 100–110.

[6] J. Salenikovich. "The racking performance of light-frame shear walls". Ph.D. dissertation. Virginia Polytechnic Institute and State University, 2000.

[7] M. He et al. "Cyclic performance of perforated wood shear walls with oversize OSB panels". In: *Journal of Structural Engineering* 125.1 (1999), pp. 10–18.

[8] James Daniel Dolan. "The dynamic response of timber shear walls". PhD diss. University of British Columbia, 1989.

[9] ASTM. *ASTM E72-77 Standard Methods of Conducting Strength Tests of Panels for Building Construction*. 1986, pp. 690–701.

[10] J.R. Tissell. "Panel-Sheathed Shear Walls – Past and Future". In: *Structural Design, Analysis and Testing, Proceedings of the Sessions Related to Design, Analysis, and Testing, Structures Congress '89*. ASCE. New York, N.Y., 1989, pp. 124–133.

[11] J.R. Tissell and J.R. Elliott. *Research Report 138, Plywood Diaphragms.* Tacoma, Washington: American Plywood Association, 1986.

[12] N.R. Adams. *Research Report 105, Plywood Shear Walls.* Tacoma, Washington: American Plywood Association, 1987.

[13] J.A. Dean, W.G. Stewart, and A.J. Carr. "The Seismic Behavior of Plywood Sheathed Shearwalls". In: *Bulletin of the New Zealand National Society for Earthquake Engineering* 19 (1986), p. 1.

[14] T. Sartori et al. "Characterization of the Mechanical Behaviour of Light-Frame Timber Shear Walls through Full-Scale Tests". In: *Proceedings of the World Conference on Timber Engineering.* Auckland, New Zealand, 2012.

[15] Q. Wang. "Relationship between Fastening Properties and Load-Deflection Response of Wood Shear Walls". M.Sc. Thesis. NB, Canada: University of New Brunswick, Faculty of Forestry and Environmental Management, 2009.

[16] B. Dolan and B. Madsen. "Monotonic and cyclic tests of timber shear walls". In: *Canadian Journal of Civil Engineering* 19.3 (1992), pp. 415–422.

[17] R. Qiang et al. "Reversed cyclic testing of high-capacity light wood frame shear walls with two and three rows of nails". In: *Engineering Structures* 304 (2024), p. 117582.

[18] R.D. Griffits. *Report on Racking Tests on Timber Framed Wall Panels Sheathed with "Asfarock" Bitumen Impregnated Insulation Board.* Tech. rep. University of Surrey, 1976.

[19] A.J. Salenikovich and J.D. Dolan. "The racking performance of shear walls with various aspect ratios. Part 2. Cyclic tests of fully anchored walls". In: *Forest Products Journal* 53 (2003), pp. 37–45.

[20] NAHB Research Center. *Cyclic Testing of Fiberboard Shear Walls with Varying Aspect Ratios.* Tech. rep. Upper Marlboro: NAHB Research Center, 2006.

[21] Z.A. Martin and T.D. Skaggs. *Shear Wall Deflection and Predictive Equations*. Tech. rep. Tacoma, Wash., US: APA Report T2001L-65, 2002.

[22] CSA. *Engineering Design in Wood. CSA O86-2014*. Toronto, ON: Canadian Standards Association, 2014.

[23] F. Kamiya et al. "Studies on wood-panel construction (I). Effect on racking resistances of bearing wall due to testing methods and wall length". In: (1981), pp. 15–38.

[24] F. Lam, H.G.L. Prion, and M. He. "Lateral resistance of wood shear walls with large sheathing panels". In: *Journal of Structural Engineering* 123 (1997), pp. 1666–1673. DOI: 10.1061/(ASCE)0733-9445(1997)123:12(1666). URL: https://doi.org/10.1061/(ASCE)0733-9445(1997)123:12(1666).

[25] Dries Byloos and Bram Vandoren. "Experimental and Analytical Assessment of the Racking Behavior of Timber Frame Walls with Single-Sided Double-Layered Sheathing Panels". In: *Engineering Structures* 316 (2024), p. 118592.

[26] Zixuan He et al. "Lateral behavior of wood frame shear wall using PVC wood-plastic composite (WPC) veneer panels". In: *Journal of Building Engineering* 89 (2024), p. 109367.

[27] D.J. Lebeda et al. "Effect of Hold-Down Misplacement on Strength and Stiffness of Wood Shear Walls". In: *Practice Periodical on Structural Design and Construction* 10.2 (2005), pp. 79–87. DOI: 10.1061/(ASCE)1084-0680(2005)10:2(79). URL: https://doi.org/10.1061/(ASCE)1084-0680(2005)10:2(79).

[28] A.R. Johnston, P.K. Dean, and H.W. Shenton. "Effects of Vertical Load and Hold-Down Anchors on the Cyclic Response of Wood Framed Shear Walls". In: *Journal of Structural Engineering* 132.9 (2006), pp. 1426–1434. DOI: 10.1061/(ASCE)0733-9445(2006)132:9(1426). URL: https://doi.org/10.1061/(ASCE)0733-9445(2006)132:9(1426).

[29] M.M. Bagheri and G. Doudak. "Experimental and Numerical Study on the Deflection of Multi-Storey Light-Frame Timber Shear Walls". In: *Engineering Structures* 233 (2021), p. 111951.

[30] D. Countryman. *Lateral Tests on Plywood Sheathed Diaphragms*. Tech. rep. 55. Tacoma, Washington, US: Douglas Fir Plywood Association Testing Laboratory, 1952.

[31] C.S. Association. *CSA O86-Engineering Design in Wood*. Mississauga: Canadian Standards Association, 2019.

[32] A. W. Council. *Special Design Provisions for Wind and Seismic*. ANSI/AWC SDPWS-2021. Leesburg, VA, 2021.

[33] D. Casagrande et al. "Analytical and Numerical Analysis of Timber Framed Shear Walls". In: *Proceedings of the World Conference on Timber Engineering*. Auckland, New Zealand, 2012.

[34] A. Filiatrault. "Static and Dynamic Analysis of Timber Shear Walls". In: *Canadian Journal of Civil Engineering* 17 (1990), pp. 643–651.

[35] A. Gupta and G. Kuo. "Wood-Framed Shear Walls with Uplifting". In: *Journal of Structural Engineering* 113 (1987), pp. 241–259.

[36] B. Folz and A. Filiatrault. "Cyclic Analysis of Wood Shear Walls". In: *Journal of Structural Engineering* 127 (2001), pp. 433–441.

[37] W. Pang and S. Hassanzadeh. "Corotational Model for Cyclic Analysis of Light-Frame Wood Shear Walls and Diaphragms". In: *Journal of Structural Engineering* 139 (2012), pp. 1303–1317. DOI: 10.1061/(ASCE)ST.1943-541X.0000595. URL: https://doi.org/10.1061/(ASCE)ST.1943-541X.0000595.

[38] T.T. Baber and M.N. Noori. "Random Vibration of Degrading, Pinching Systems". In: *Journal of Engineering Mechanics* 111.8 (1985), pp. 1010–1026.

[39] Jian Xu and J. Daniel Dolan. "Development of Nailed Wood Joint Element in ABAQUS". In: *Journal of Structural Engineering* 135.8 (2009), pp. 968–976.

[40] W. Seim et al. “OSB and GFB as Sheathing Materials for Timber-Framed Shear Walls: Comparative Study of Seismic Resistance”. In: *Journal of Structural Engineering* 142 (2016), E4015004.

[41] J. Judd and F. Fonseca. “Analytical Model for Sheathing-to-Framing Connections in Wood Shear Walls and Diaphragms”. In: *Journal of Structural Engineering* 131 (2005), pp. 345–352. DOI: `10.1061/(ASCE)0733-9445(2005)131:2(345)`. URL: `https://doi.org/10.1061/(ASCE)0733-9445(2005)131:2(345)`.

[42] Dassault Systèmes Simulia Corp. *ABAQUS*. Computer software, Version 2020. 2020.

[43] Instituto Nacional de Normalización. *NCh 1198: Madera - Construcciones en Madera - Cálculo*. 2014.

[44] Sardar Malekmohammadi et al. “Analytical Micromechanics Equations for Elastic and Viscoelastic Properties of Strand-Based Composites”. In: *Journal of Composite Materials* 48.15 (2014), pp. 1857–1874.

[45] Sardar Malek et al. “Strain-Softening Response and Failure Prediction in Notched Oriented Strand Board”. In: *Journal of Materials in Civil Engineering* 31.6 (2019), p. 04019094.

[46] R.J. Ross. *Wood Handbook: Wood as an Engineering Material*. USDA Forest Service, 2021.

[47] A. Jara and F. Benedetti. *Informe No. 14 – Registro de Estudio de Ensayos de Conectores*. Tech. rep. Concepción, Chile: University of the Bío Bío, 2017.

[48] Dina Ghazi-Nader et al. “Deflection of Wood-Frame Shear Walls Under Large Lateral Loads: Analytical Design Equations Versus Experimental Data”. In: *Proceedings of the Canadian Society of Civil Engineering Annual Conference*. Cham: Springer International Publishing, 2023, pp. 851–865.

[49] APA - The Engineered Wood Association. *Panel Design Specification*. Tacoma, WA, 2020.

[50] S. Malekmohammadi et al. “Analytical micromechanics equations for elastic and viscoelastic properties of strand-based composites”. In: *Journal of Composite Materials* 48.15 (2014), pp. 1857–1874.

[51] G. Foliente. “Stochastic dynamic response of wood structural systems”. PhD thesis. Blacksburg, VA: Virginia Polytechnic Institute and State University, 1993.

[52] Jian Xu. “Development of a general dynamic hysteretic light-frame structure model and study on the torsional behavior of open-front light-frame structures”. In: *Vol. 68, no. 02* (2006).

[53] H. Krawinkler et al. *Development of a testing protocol for woodframe structures.* CUREE Report W-02, Task 1.3.2. Richmond, CA: Consortium of Universities for Research in Earthquake Engineering (CUREE), 2001.

A Appendix: Orthotropic Material Investigation

This appendix presents the results of an investigation into the effect of material orientation of wood members on the results for beam and solid elements, to determine if orthotropic material properties can be applied to these elements. As is well known, wood is an orthotropic material, meaning it has different mechanical properties in three distinct directions (as shown in Figure A-1). To accurately capture the performance of wood in finite element (FE) modeling, it is essential to use orthotropic material properties. Therefore, two shear wall models were created: one with beam and shell elements, and another with solid elements, assigning orthotropic properties to the frame members as shown in Figures A-2 and A-3, respectively. The primary material direction (1-direction or longitudinal direction) was aligned with the length or width of the studs. The material properties of the wood are provided in Table A-1.

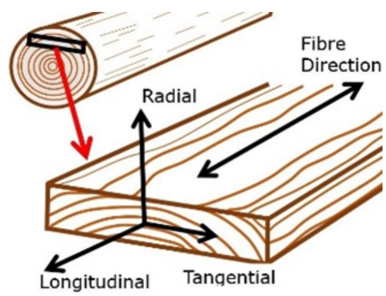

Figure A-1: Three perpendicular directions of wood as an orthotropic material.

Table A-1: Material Properties for radiata pine framing and 11.1-mm-thick OSB panels used as input data for ABAQUS [3, 4, 44–46].

Material Property	**Framing members (GPa)**	**OSB (GPa)**
E1	11.4	5.17
E2	1.2	2.98
E3	0.75	0.13
G12	0.869	1.255
G13	0.797	1.307
G23	0.142	0.128
ν_{12}	0.467	0.184
ν_{13}	0.456	0.364
ν_{23}	0.488	0.312

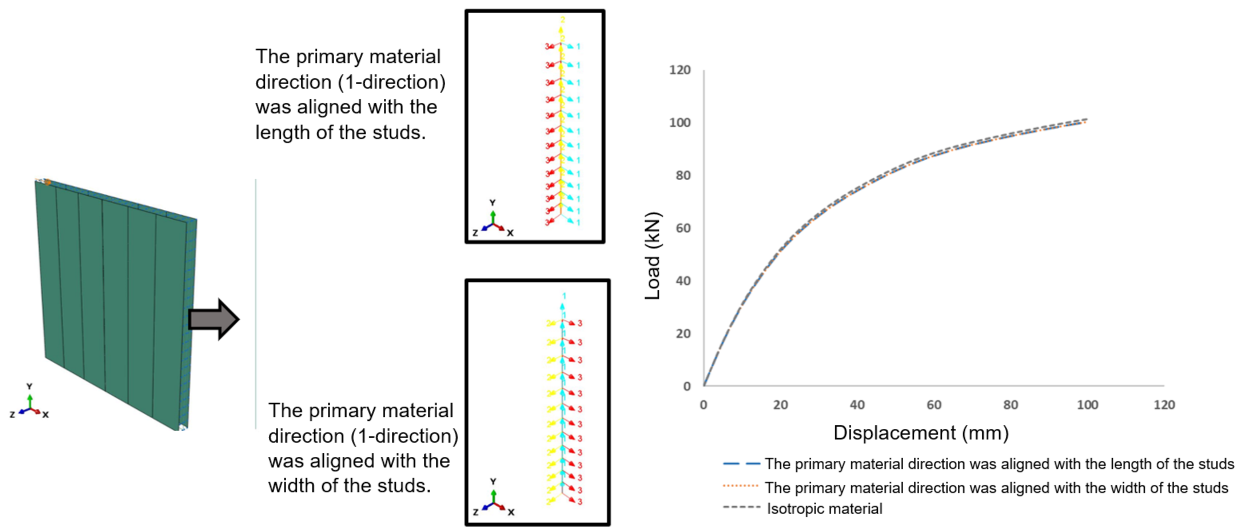

Figure A-2: Load-displacement results of the shear wall using beam and shell elements with different material orientations of the frame members.

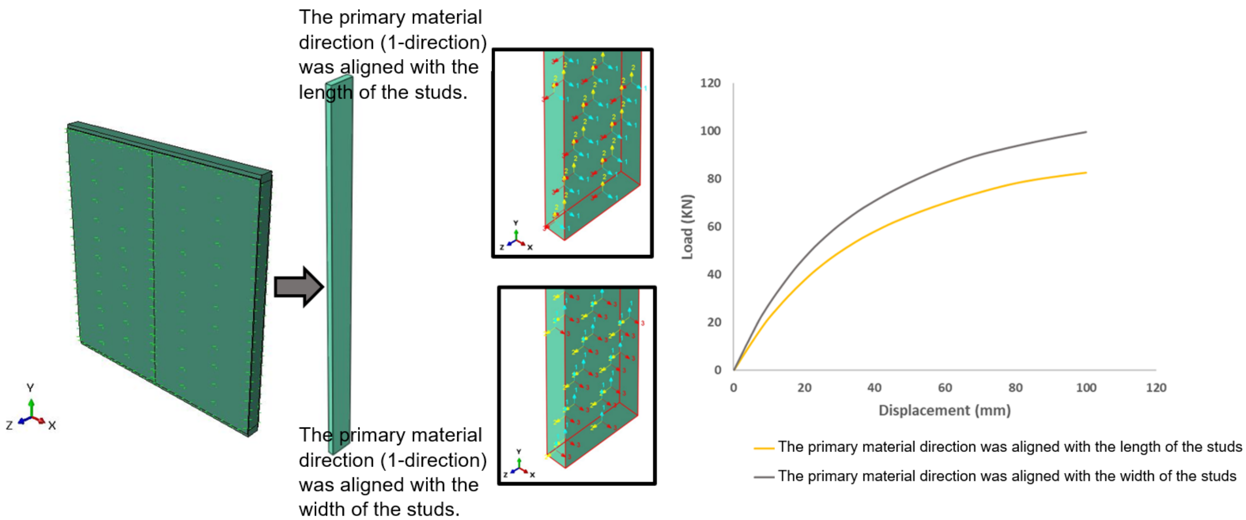

Figure A-3: Load-displacement results of the shear wall using solid elements with different material orientations of the frame members.

As the results indicate, the studs modeled with beam elements, regardless of material orientation, produced similar outcomes. This suggests that beam elements (B31) in ABAQUS cannot accurately capture the orthotropic properties of the material, functioning instead as isotropic. In contrast, the model with solid elements (C3D8R) showed differing results, with higher strength observed when the primary material direction was aligned with the length of the studs. Therefore, it can be concluded that orthotropic material properties are effectively captured by solid elements, but not by beam elements.

B Appendix: Lateral Monotonic Response

This appendix presents the deflection response calculated using the equations provided in the American Wood Council (AWC) Special Design Provisions for Wind and Seismic (SDPWS) and the Canadian Standards Association (CSA O86) for additional shear wall specimens. Further details and results are available in our previous study [48].

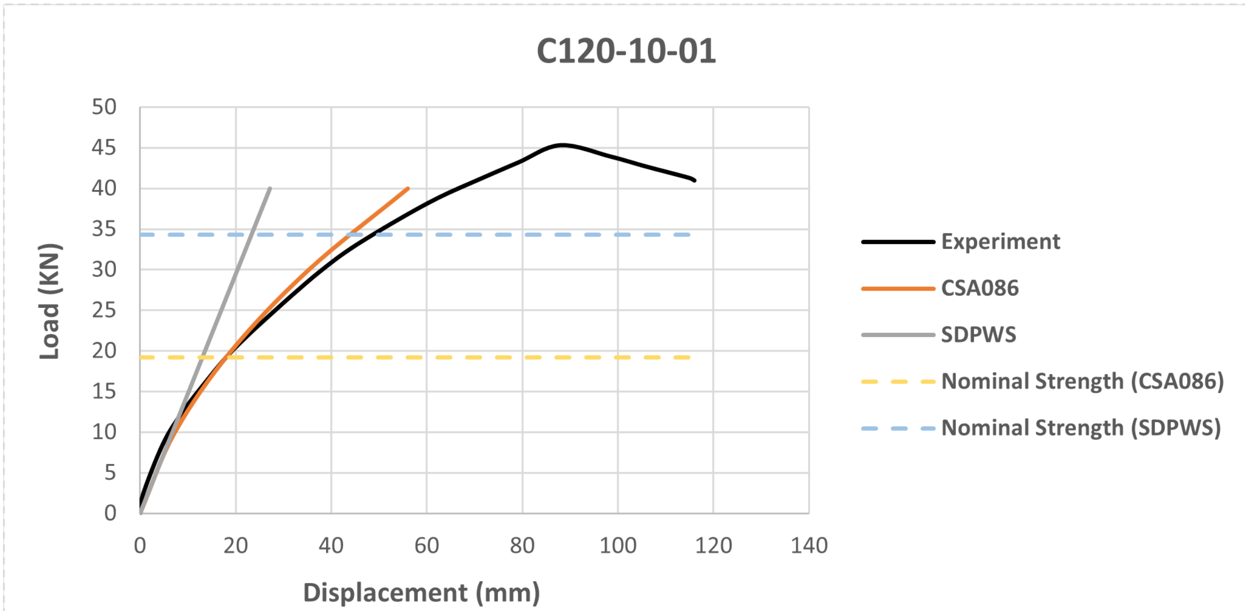

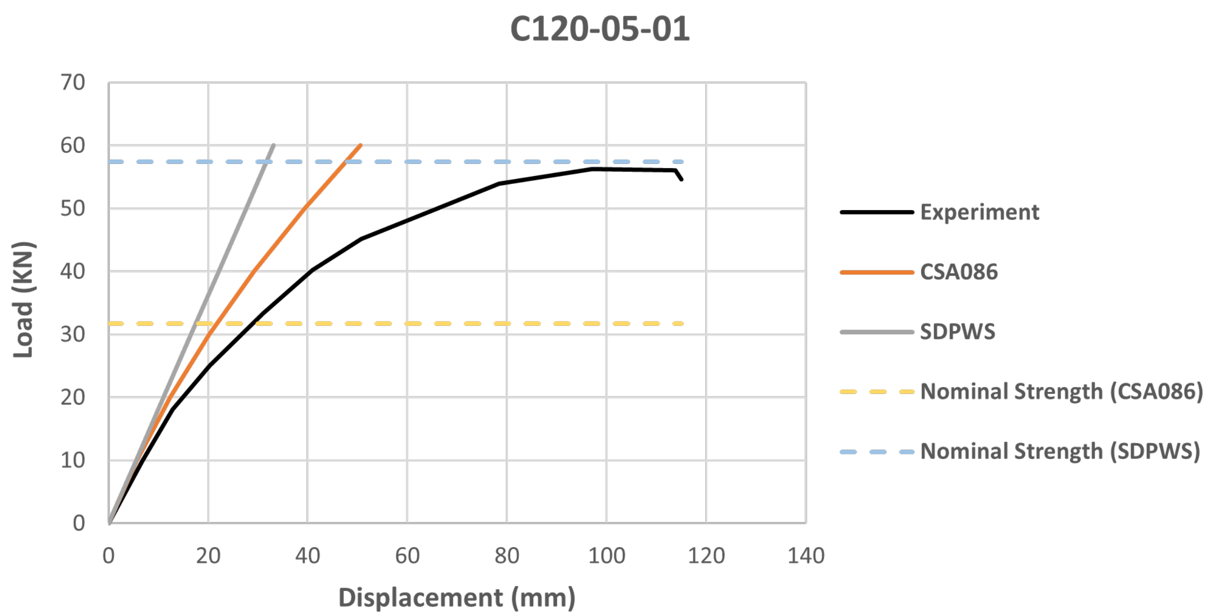
C120-05-01
Load (KN)
Displacement (mm)
0
10
20
30
40
50
60
70
0
20
40
60
80
100
120
140
Experiment
CSA086
SDPWS
Nominal Strength (CSA086)
Nominal Strength (SDPWS)

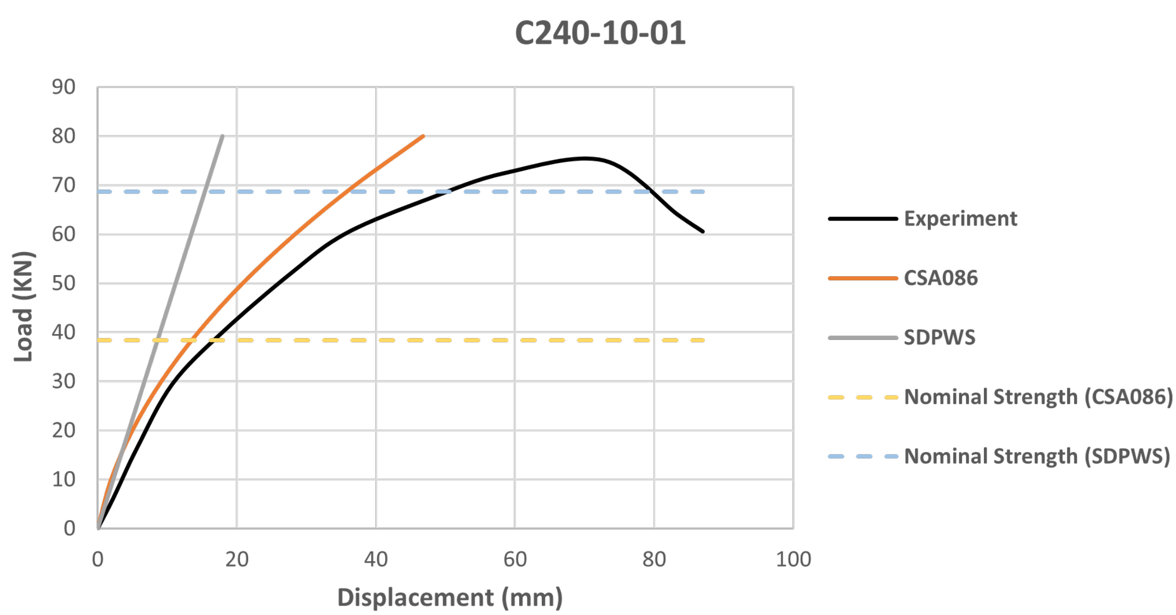
C240-10-01
Load (KN)
Displacement (mm)
0
10
20
30
40
50
60
70
80
90
0
20
40
60
80
100
Experiment
CSA086
SDPWS
Nominal Strength (CSA086)
Nominal Strength (SDPWS)

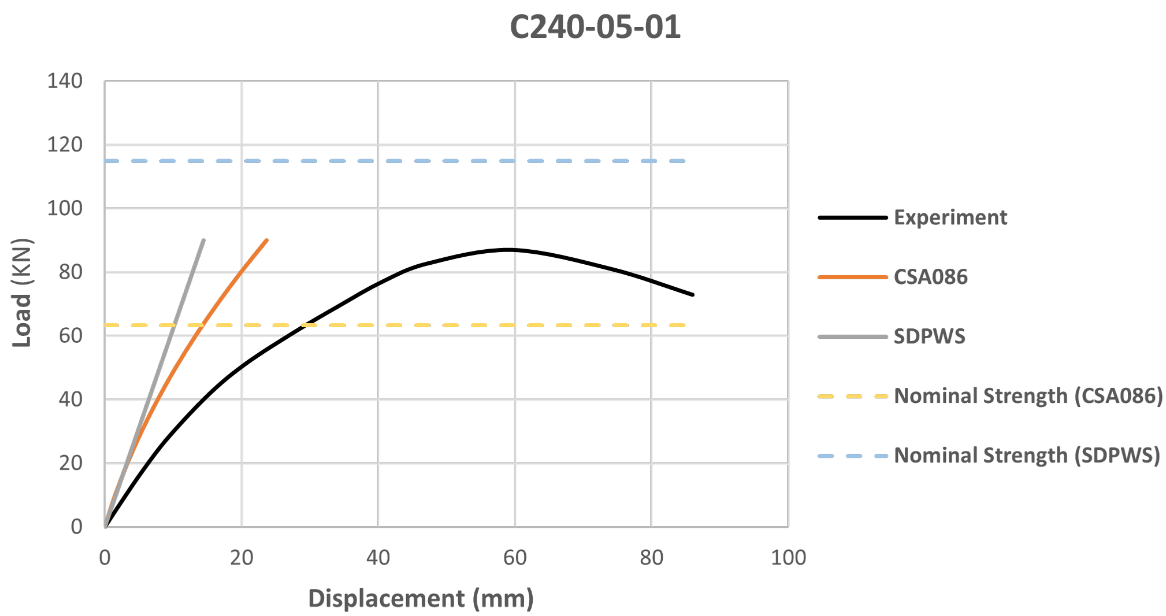
C240-05-01
140
120
100
80
60
40
20
0
Load (KN)
0
20
40
60
80
100
Displacement (mm)
Experiment
CSA086
SDPWS
Nominal Strength (CSA086)
Nominal Strength (SDPWS)

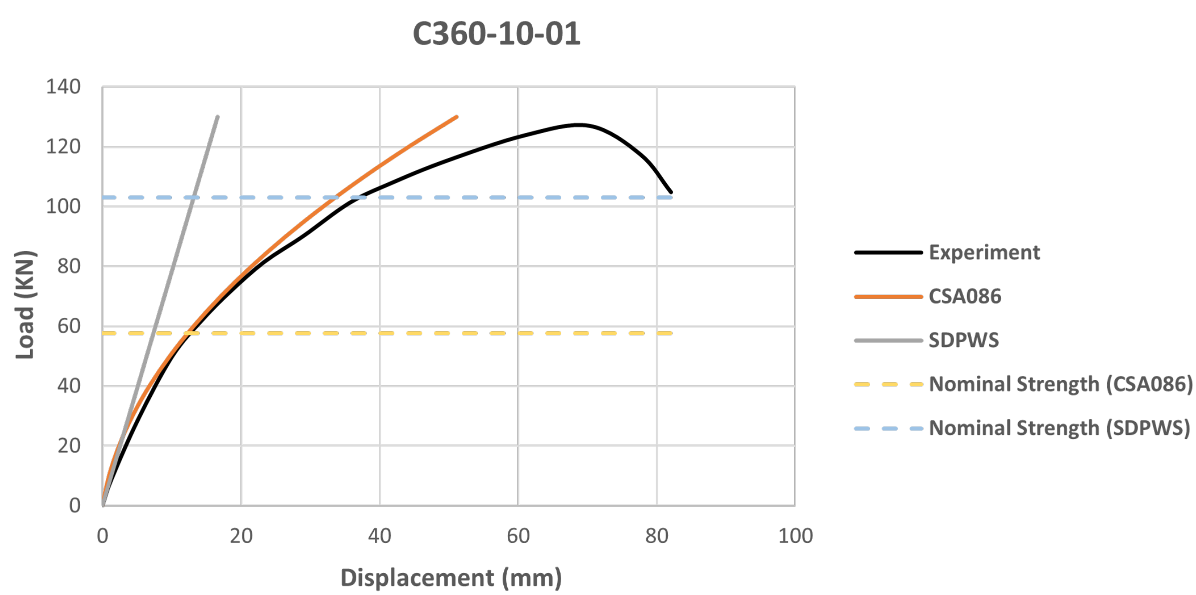
C360-10-01
140
120
100
80
60
40
20
0
Load (KN)
0
20
40
60
80
100
Displacement (mm)
Experiment
CSA086
SDPWS
Nominal Strength (CSA086)
Nominal Strength (SDPWS)

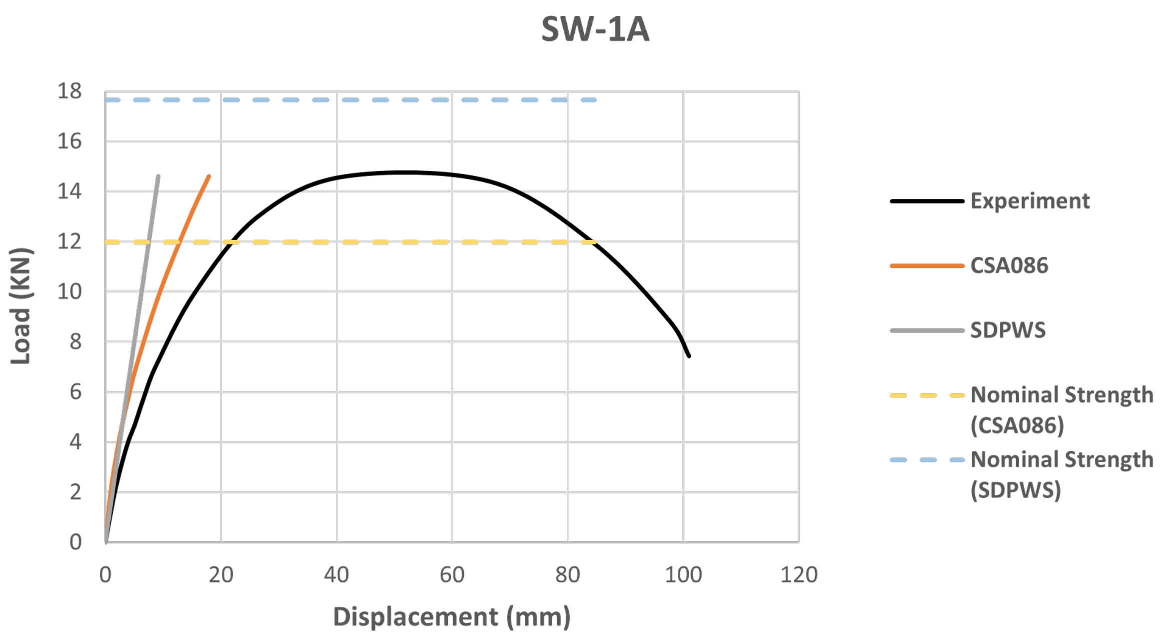
SW-1A
Load (KN)
18
16
14
12
10
8
6
4
2
0
0
20
40
60
80
100
120
Displacement (mm)
Experiment
CSA086
SDPWS
Nominal Strength (CSA086)
Nominal Strength (SDPWS)

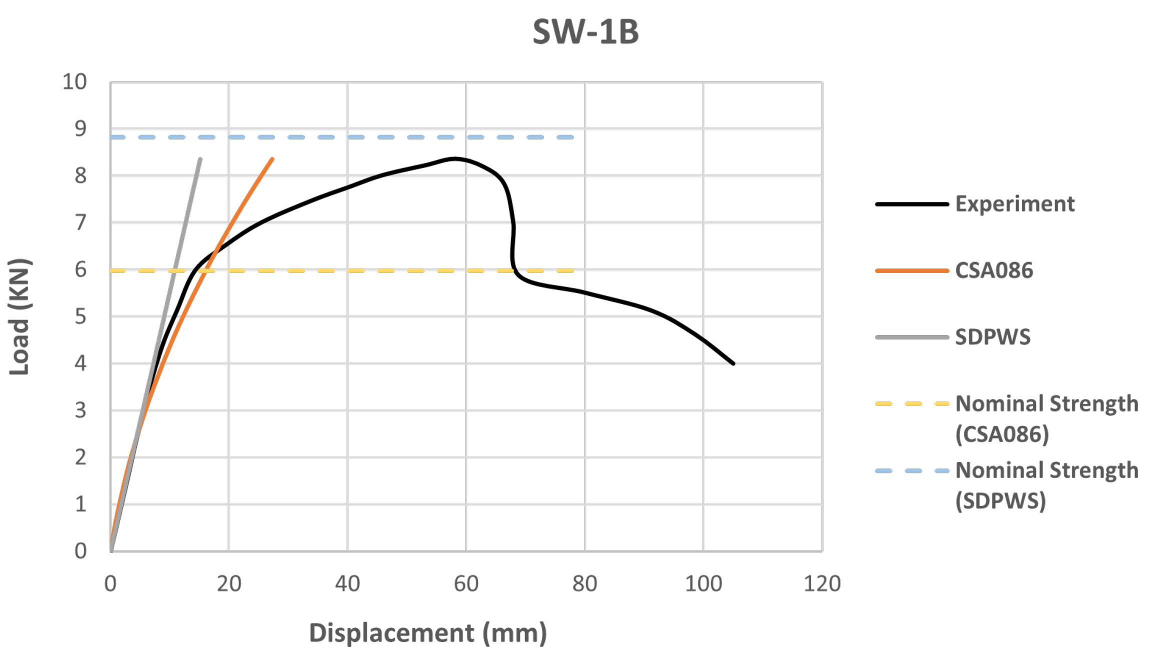
SW-1B
Load (KN)
10
9
8
7
6
5
4
3
2
1
0
0
20
40
60
80
100
120
Displacement (mm)
Experiment
CSA086
SDPWS
Nominal Strength (CSA086)
Nominal Strength (SDPWS)

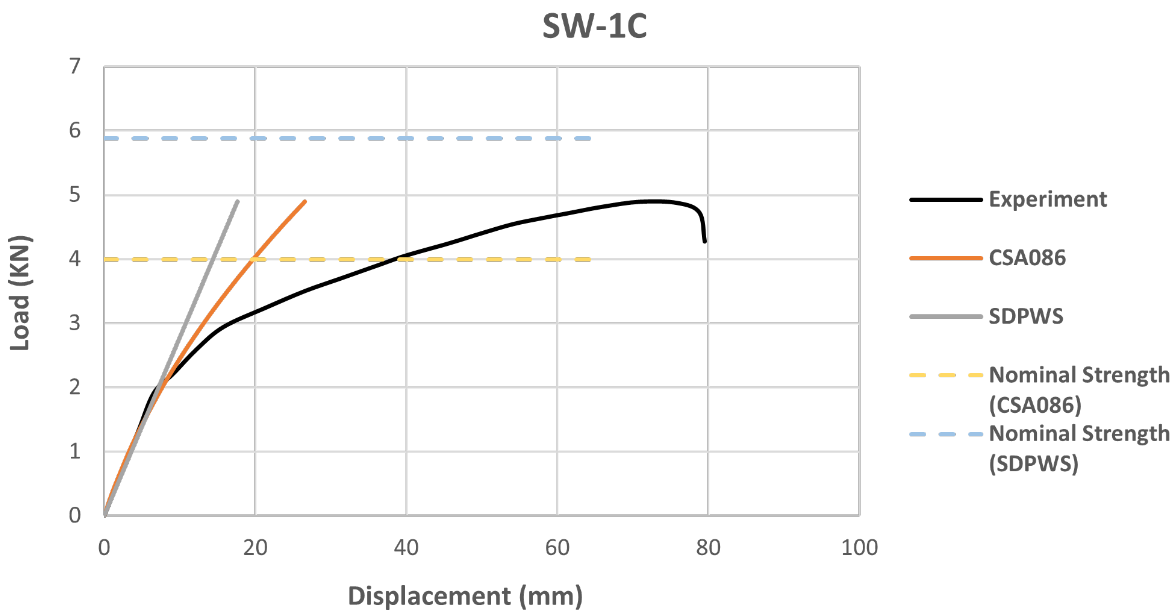
SW-1C
Load (KN)
Displacement (mm)
0
1
2
3
4
5
6
7
0
20
40
60
80
100
Experiment
CSA086
SDPWS
Nominal Strength (CSA086)
Nominal Strength (SDPWS)

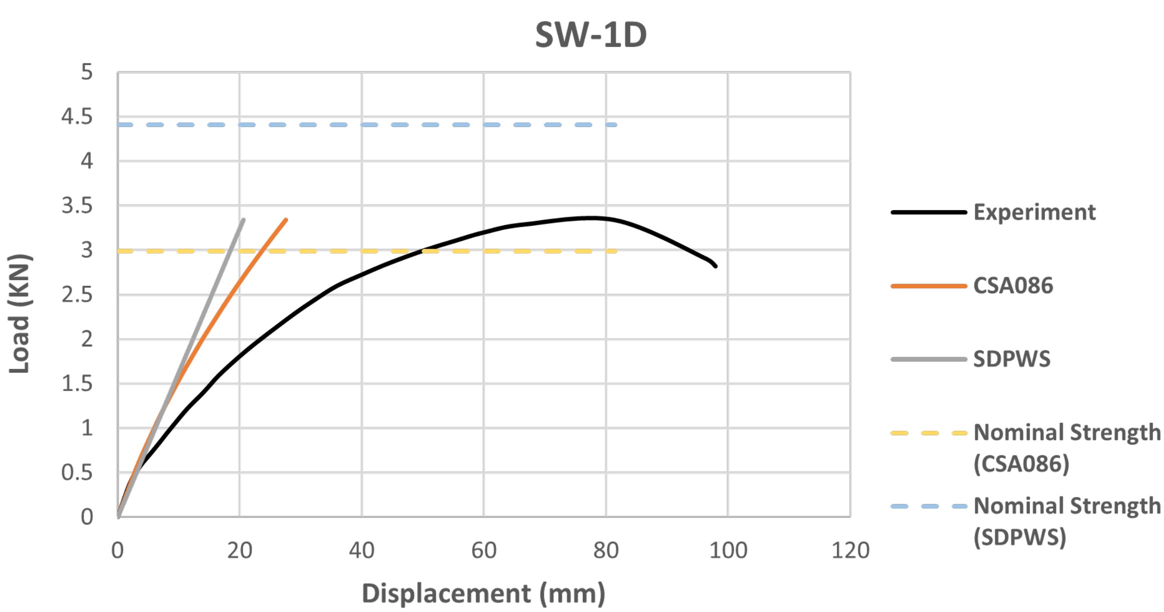
SW-1D
Load (KN)
Displacement (mm)
0
0.5
1
1.5
2
2.5
3
3.5
4
4.5
5
0
20
40
60
80
100
120
Experiment
CSA086
SDPWS
Nominal Strength (CSA086)
Nominal Strength (SDPWS)